AD-A152 659 THE WEIGHTING FUNCTION FOR SCINTILLATION ON A FOLDED PATH(U) NAVAL POSTGRADUATE SCHOOL MONTEREY CA B G AN DEC 84 1/1

UNCLASSIFIED F/G 20/6 NL

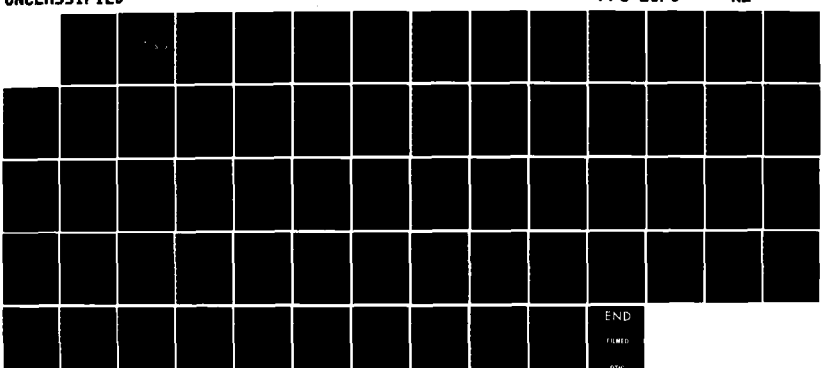

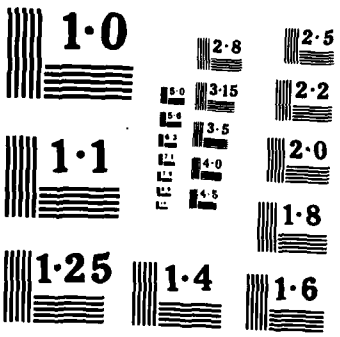
1·0
1·1
1·25
1·4
1·6
1·8
2·0
2·2
2·5
2·8
3·15
3·5
4·0
4·5

(2)

NAVAL POSTGRADUATE SCHOOL
Monterey, California

THESIS

THE WEIGHTING FUNCTION
FOR SCINTILLATION ON A FOLDED PATH

by

BYUNG G. AN

December 1984

Thesis Advisor: E. A. Milne

Approved for public release; distribution unlimited.

SECURITY CLASSIFICATION OF THIS PAGE *(When Data Entered)*

REPORT DOCUMENTATION PAGE	READ INSTRUCTIONS BEFORE COMPLETING FORM
1. REPORT NUMBER	2. GOVT ACCESSION NO. A152 659 / 3. RECIPIENT'S CATALOG NUMBER
4. TITLE *(and Subtitle)* The Weighting Function for Scintillation on a Folded Path	5. TYPE OF REPORT & PERIOD COVERED Master Thesis; December 1984
	6. PERFORMING ORG. REPORT NUMBER
7. AUTHOR(s) Byung G. AN	8. CONTRACT OR GRANT NUMBER(s)
9. PERFORMING ORGANIZATION NAME AND ADDRESS Naval Postgraduate School Monterey, California 93943	10. PROGRAM ELEMENT, PROJECT, TASK AREA & WORK UNIT NUMBERS
11. CONTROLLING OFFICE NAME AND ADDRESS Naval Postgraduate School Monterey, California 93943	12. REPORT DATE December 1984
	13. NUMBER OF PAGES 63
14. MONITORING AGENCY NAME & ADDRESS *(if different from Controlling Office)*	15. SECURITY CLASS. *(of this report)* Unclassified
	15a. DECLASSIFICATION/ DOWNGRADING SCHEDULE

16. DISTRIBUTION STATEMENT *(of this Report)*

Approved for public release; distribution unlimited

17. DISTRIBUTION STATEMENT *(of the abstract entered in Block 20, if different from Report)*

18. SUPPLEMENTARY NOTES

19. KEY WORDS *(Continue on reverse side if necessary and identify by block number)*

Scintillation Path Weighting

20. ABSTRACT *(Continue on reverse side if necessary and identify by block number)*

In the case of a spherical beam wave propagating in a weakly inhomogeneous medium which has a Kolmogorov spectrum, Dr. Ze'evi derived a weighting function for scintillation for a direct and for a folded path with respect to the position of the turbulent medium. Experiments were performed to verify Ze'evi's weighting function for a folded path for three different types of reflectors. The experimental

DD FORM 1 JAN 73 1473 EDITION OF 1 NOV 65 IS OBSOLETE

S N 0102-LF-014-6601

SECURITY CLASSIFICATION OF THIS PAGE *(When Data Entered)*

results did not support Dr. Ze'evi's threory. We found that the scintillation weighting functions are less weighted near the detector and have an unexpected increase near the reflector. These results are discussed by using a geometric optical model of the turbulence.

Approved for public release; distribution is unlimited.

The Weighting Function for Scintillation on a Folded Path

by

Byung G. An
Ltcol, Korea Air Force
B.S., Korea Air Force Academy, 1972

Submitted in partial fulfillment of the requirements for the degree of

MASTER OF SCIENCE IN PHYSICS

from the

NAVAL POSTGRADUATE SCHOOL
Dec 1984

Author: Byung G. An
Byung G. An

Approved by: Edmund A. Milne
E.A. Milne, Thesis Advisor

D.L. Walters, Second Reader

Gordon E. Schacher, Chairman,
Department of Physics

John N. Dyer,
Dean of Science and Engineering

ABSTRACT

In the case of a spherical beam wave propagating in a weakly inhomogeneous medium which has a Kolmogorov spectrum, Dr. Ze'evi derived a weighting function for scintillation for a direct and for a folded path with respect to the position of the turbulent medium. Experiments were performed to verify Ze'evi's weighting function for a folded path for three different types of reflectors. The experimental results did not support Dr. Ze'evi's theory. We found that the scintillation weighting functions are less weighted near the detector and have an unexpected increase near the reflector. These results are discussed by using a geometric optical model of the turbulence.

TABLE OF CONTENTS

LIST OF FIGURES

ACKNOWLEDGEMENT

The author would like to express his sincere appreciation to Professor E. A. Milne, for his patient, ever present guidance and direction. Without his instruction in scintillation experimental procedure the completion of this project would not have been possible.

The guidance of Professor D. L. Walters was really invaluable in the analysis of the work.

The author wishes to dedicate this thesis to his parents and to his wife, Jeong Sook, for their constant love.

I. INTRODUCTION

When optical radiation passes through the atmosphere the amplitude and phase characteristics of the beam are altered by the inhomogeneity of the index of the refraction along the propagation path. These effects limit the performance of laser communication and radar systems. It is, therefore, important to have a theory for predicting the nature of the propagation of the light beam in a random medium.

Dr. Ze'evi [Ref.1] in his doctoral thesis developed a weighting function for the scintillation of a spherical wave over a folded path. To verify Ze'evi's function many experiments were attempted by Speer and Parker [Ref.2], Constantine [Ref.3], Flenniken [Ref.4], and Henry [Ref.5].

Essentially our work was divided into three parts. The first part was the characterization of turbulence in the turbulence chamber and the second part was the measurement of the experimental weighting function for the folded path. The third part was to compare the experimental results to the Ze'evi's weighting function and to describe the results of the effects of the geometric optical model of turbulence.

In this paper we concentrated on the third part. The first and the second parts will be discussed in detail in the papers of Mr. Lee [Ref.6] and of Mr. Kim [Ref.7] respectively.

We first review the development of Dr. Ze'evi's weighting function for the folded path and discuss briefly the experimental procedure. Then, we discuss the effects of the geometrical-optic model of a turbulent medium.

II. THEORETICAL BACKGROUND

Here, we will first outline the theory of the index of refraction fluctuations and then review the log-amplitude variance and finally Ze'evi's folded path theory.

A. INDEX OF REFRACTION

In optical propagation through the atmosphere, the fluctuations of refraction index are sufficient to produce beam wander, beam spread, and intensity fluctuations. The refractive index is assumed to be a real function of the temperature and the pressure, and has the following form [Ref.8]:

$$n(r) = 1.0 + \frac{77.6}{T(r)} P(r) \left(1 + \frac{.0075}{\lambda^2}\right) \times 10^{-6}, \qquad \text{(eqn 2.1)}$$

where n(r) = real refraction index at a point r,
T(r) = Temperature (Kelvin),
P(r) = Pressure (Millibar),
λ = Beam wavelength (micrometer).

The dependence of the refractive index of the atmosphere on the change in P and T is given by the differential of equation 2.1

$$dn = 77.6 \frac{P}{T} \left(\frac{dP}{P} - \frac{dT}{T}\right) \left(1 + \frac{.0075}{\lambda^2}\right) \times 10^{-6} \qquad \text{(eqn 2.2)}$$

Since the pressure fluctuations are relatively small, the fluctuations of the refraction index are governed by temperature fluctuations. An accepted measure of the strength of turbulence in the atmosphere is the refractive

G. DATA REDUCTION SYSTEM

The output of the log converter, the clock pulse of the chopper wheel, and the amplified temperature fluctuation signal were transfered to the DATA-6000 waveform analyzer. We used a Model-610 plug-in module which has sampling rates up to 100,000 per second. A HP 9825A calculator was programmed to calculate the standard deviation of the amplified temperature fluctuations and of the log intensities.

We made five separate runs at each turbulence chamber location and each run consisted of 500 samples. The temperature structure constant, C_t^2, and the log intensity variance were then calculated from these data by the HP 9825A calculator.

The HP 9825A calculator functioned as the controller and input-output device to the DATA-6000, HP 9862A plotter, and HP 9871A printer.

The experimental set up for the folded path is shown in Figure 3.4. A laser beam from a single mode He-Ne gas laser (λ= 6328Å) was used as a source. The laser beam was chopped by a mechanical chopper wheel with an open to closed ratio of 1:4. The chopper wheel rotated at 3000 rpm and provided a pulse rate of one KHz. The chopped beam was then directed to the target reflector by a beam spliter.

We employed a corner cube, flat mirror and a cat's eye as the target reflector and concentrated on the comparison of the scintillation results from the different reflectors.

The optical scintillation was detected by an RCA #30827 Silicon Avalanche Photodiode. When operated at 250 volts, the detector provided extremely high signal to noise ratio without the need for cooling. We did not use any spectral filters as all of our experimental work was done inside the tunnel at night.

The output from the detector was amplified by a PAR model 113 amplifier. The high and low frequency roll-offs were set to allow the signal to be amplified without creating any distortions of the signal.

F. DATA PROCESSING EQUIPMENT

The signals amplified by the PAR #113 were passed to the demodulator. This device sampled an incoming signal and held its instantaneous maximum signal level for the desired duration. The background was then sampled and the difference of these two levels was taken. This difference was held constant until the next difference was measured. The reconstructed signal was then passed to a log convertor.

The log-convertor produced an output voltage that was proportional to the log of the input voltage.

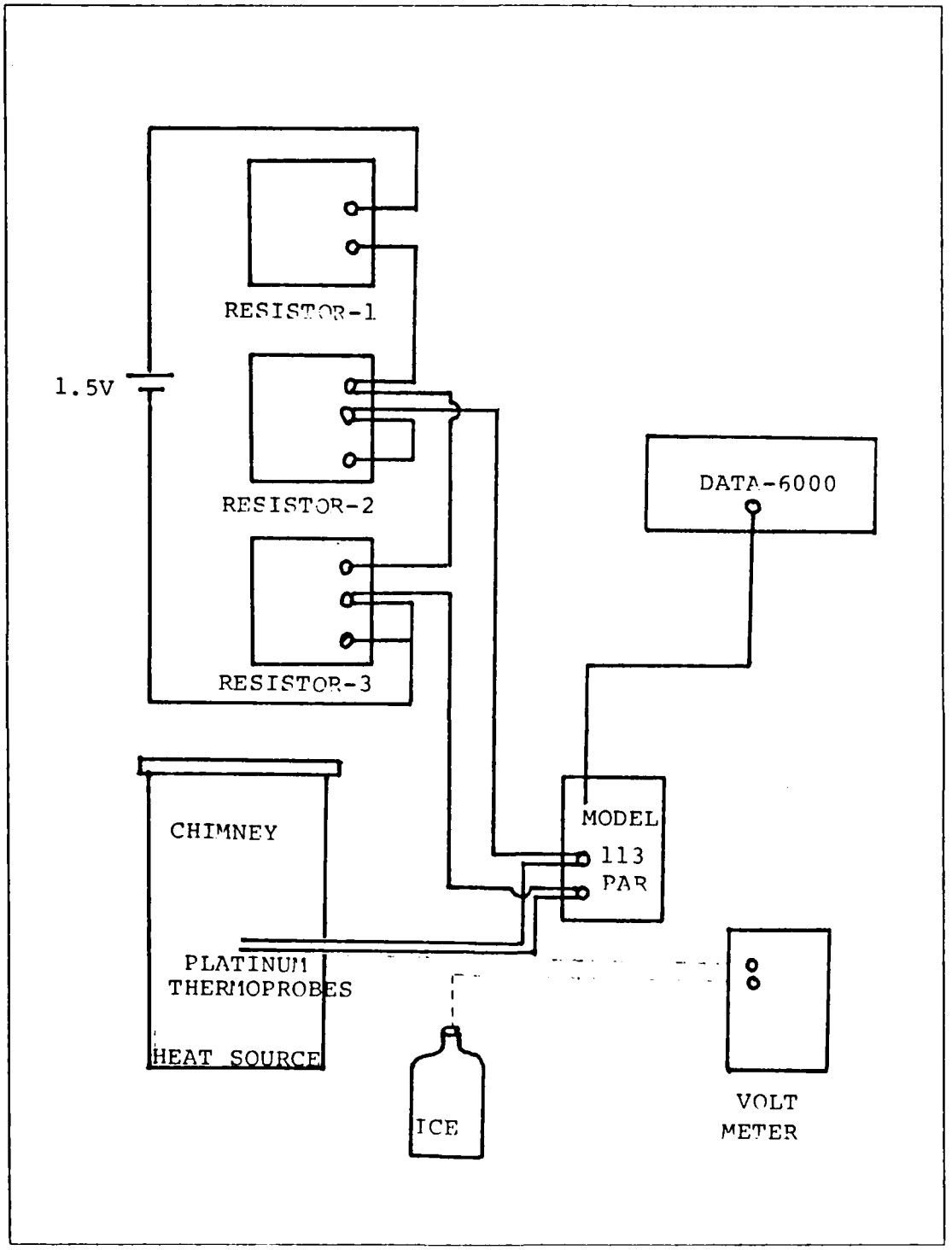

Figure 3.3 Schematic of AC Bridge System.

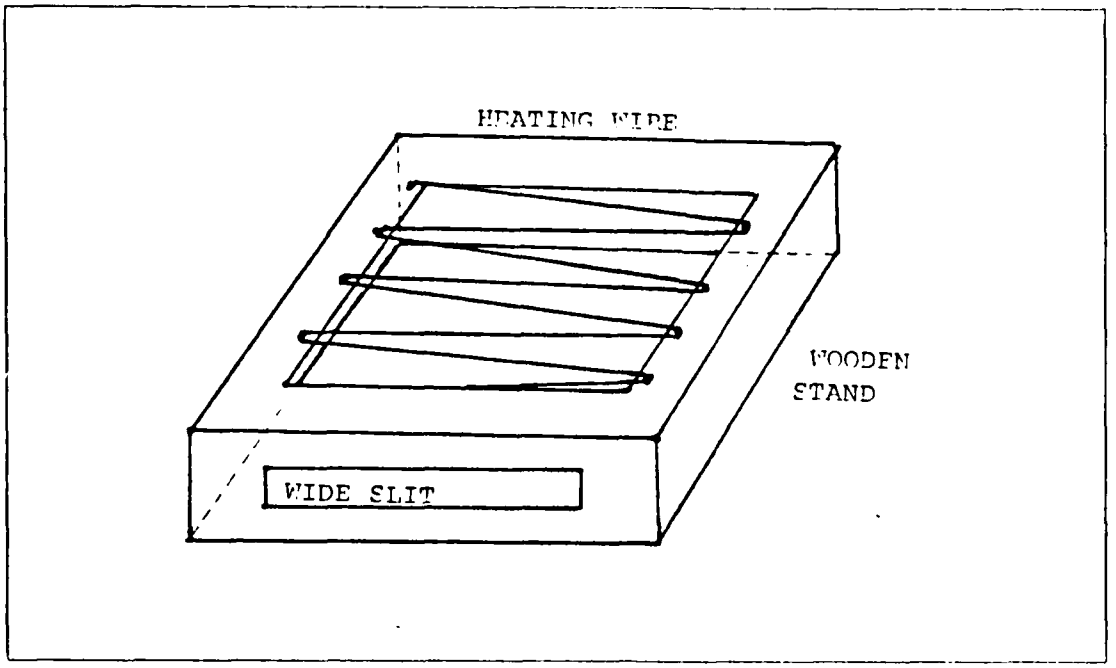

Figure 3.2 Heat Source.

platinum-resistance temperature-probes separated by 6 centimeter. A schematic of the AC bridge system is shown in Figure 3.3.

The resistance of the platinum probes varied in proportion to the temperature changes in the turbulent medium. The varying resistance produced the voltage difference in the bridge. The fluctuations of the voltage difference in the bridge were amplified using a Princeton Applied Research model 113 Amplifier then fed to a DATA-6000 waveform analyzer. The DATA-6000 then calculated the temperature structure parameter.

E. OPTICAL EQUIPMENT

We only measured the weighting function for the folded path since the direct path scintillation is thought to be well explained by the theory.

installed a fan rotating at one Hz under the heating wire to break the convective laminar flow into turbulent flow.

The whole process for the turbulence is as follows: The exterior air comes into a side slit and is then heated by the heating wire. The heated air is broken up into a turbulent flow by the fan and is drawn upward through the beam path by the upper exhaust fan.

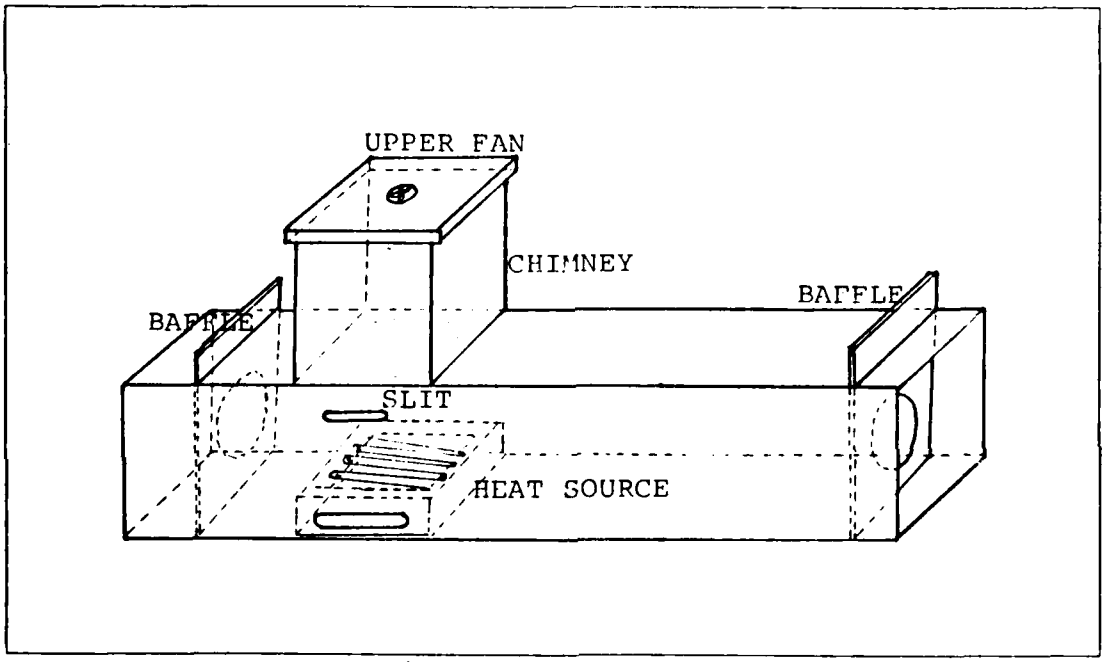

Figure 3.1 Turbulence Chamber.

D. TURBULENCE MEASUREMENT EQUIPMENT

For getting some quantitative measure of the turbulence present, the temperature structure constant, C_t^2 was measured at each path position of the turbulence section during the experimental run. The C_t^2 was measured using two

B. TUNNEL AND TURBULENCE CHAMBER

We used the same tunnel that was constructed by Constantine [Ref.3] and Flenniken [Ref.4]. The tunnel is 61 meters long by .61 meter wide by .61 meter high and consisted of 25 sections 2.4 meters long. The tunnel was treated with a water sealant, painted white on the exterior and flat black on the interior to eliminate reflection.

The turbulence chamber was made by modifying a tunnel section. It could be placed at any desired location along the 61 meter tunnel. Figure 3.1 shows the turbulence chamber. A .64 meter high chimney was constructed over the opening of the tunnel and a fan was installed in the chimney cover to create a positive air flow upward through the beam. Above the optical path a small slit was cut in the side of the turbulence chamber to insert the platinum-resistance temperature-probes into the region of turbulence. To allow airflow in under the heat source, a wide slit was cut just below the heating wire. Both of the holes were baffled to prevent unwanted airflow at the turbulence region. In addition, two plywood baffles were installed inside the tunnel on both sides of the heat source to reduce the longitudinal airflow as much as possible. These baffles had a hole cut of sufficient size to allow laser beam propagation without obscuring the laser beam.

C. HEAT SOURCE

The heat source is shown in Figure 3.2. The heating wire was installed on a wooden stand with ceramic insulators in a series of "V"s. It was connected to a variac for providing the desired voltage.

The wooden stand was reconstructed so that its width was the same as the interior width of the turbulence chamber and the height of the stand was lowered. Additionally we

III. EXPERIMENTAL APPROACH

A. BACKROUND

Because of several previous attempts to prove Ze'evi's weighting function for the folded path, most of the equipment to perform the experiment were available. We made only minor modifications to the turbulence chamber that was used in the earlier experiments.

To verify Ze'evi's theory, the turbulence in the turbulence chamber must be in the Kolmogorov inertial subrange region and needs to be as uniform as possible at each of the different locations along the beam path. To verify the existence of a Kolmogorov structure function, the turbulence chamber was first assembled in the basement of Spanagel Hall and then tested. After setting the experimental system on the roof of Spanagel Hall the turbulence chamber was tested again and the results compared to those measured in the basement [Ref.6].

During the experiment, we measured C_t^2 to normalize the experimental results at the different locations along the beam propagation path. Additionally the optical system had to be isolated from the outside disturbances. For this reason, we sealed the tunnel with masking tape and the optical equipment were also sealed under the tables at the end.

With these considerations in mind, we will discuss the entire experimental set up.

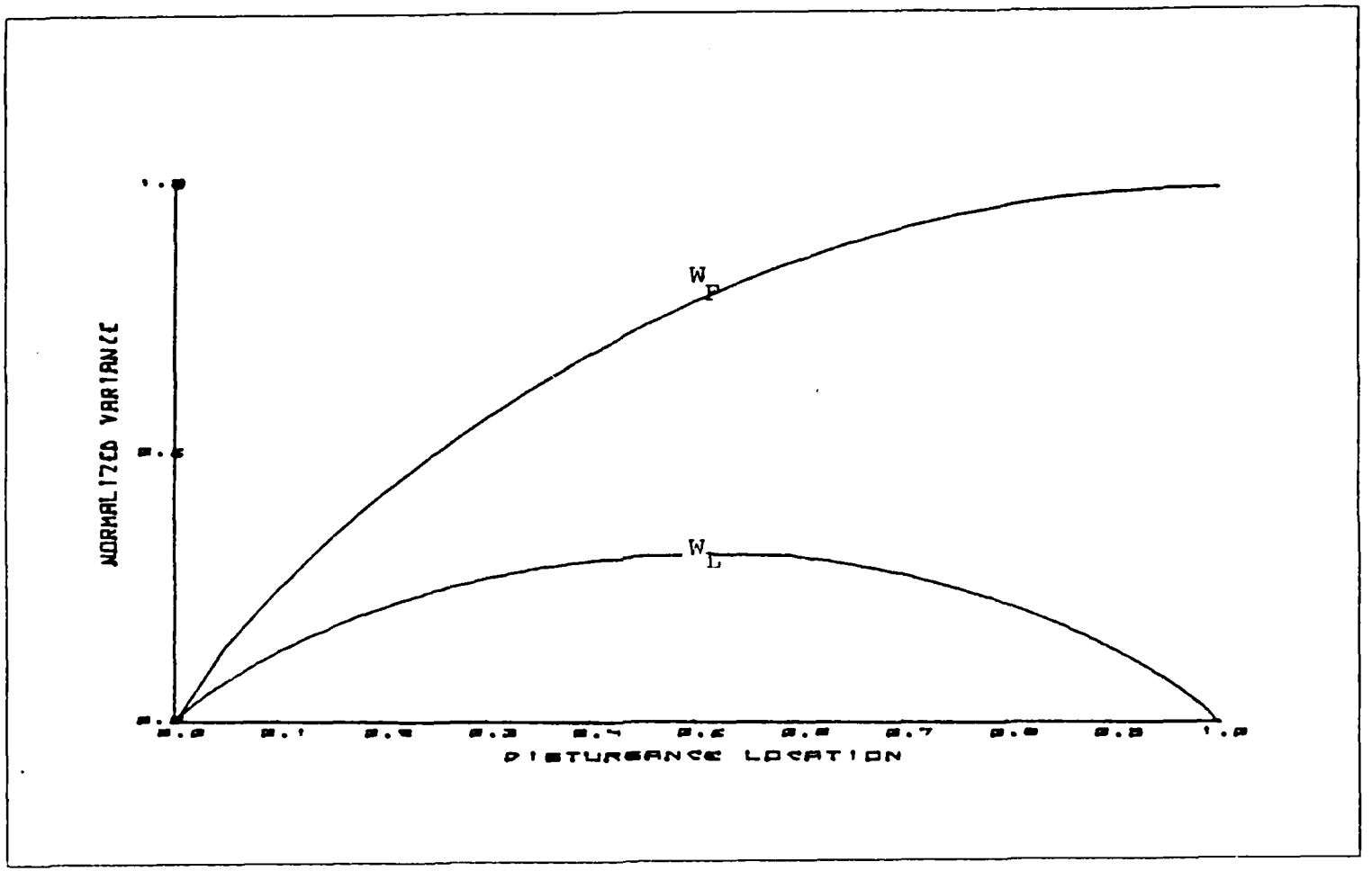

Figure 2.2 Ze'evi's Weighting Function of Spherical Waves for a Direct Path (W_L) and for a Folded Path (W_F).

$$\sigma_\chi^2(L) = A_2 C_n^2 \int_0^L dZ \left[\frac{Z(L-Z)}{L}\right]^{5/6}, \qquad \text{(eqn 2.16)}$$

where $A = .033(-4)\,\Gamma(-5/6)\cos(5\pi/12)\,\pi^2 k^{7/6} = 2^{-7/6} A_1$.

Taking " X = Z/L " then

$$\sigma_\chi^2(L) = A_2 L^{11/6} C_n^2 \int_0^1 dX [X(1-X)]^{5/6} \qquad \text{(eqn 2.17)}$$

Dr. Ze'evi proposed the path weighting functions for the spherical wave by regarding C_n^2 as constance, these are

Direct path : $W_L(X) = [X\,(\,1-X\,)]^{5/6}$,

Folded path : $W_F(X) = [X\,(\,2-X\,)]^{5/6}$,

where X = Z/L,

Z = turbulence location from the detector,

L = pathlength.

The two functions are shown in Figure 2.2. As we can see from Figure 2.2, the main contribution for the folded path comes from the vicinity of the target mirror.

He derived the weighting function from the log intensity equation of a spherical wave for the folded path using the results of Smith [Ref.11]. The log intensity equation for the folded path is

$$\sigma_\chi^2(F,\theta=0) = 64\pi^2k^2\int_0^1 dz\int_0^\infty K\phi(K)\sin^2\left(\frac{K^2z(2L-z)}{4kL}\right)dK, \quad \text{(eqn 2.12)}$$

where k = wave number ($2\pi/\lambda$),
$\phi(K)$ = the isotopic form of the Fourier transform of the refractive index covariance function,
Z = path location,
K = two dimensional spatial wave number, of turbulence (= $2\pi/L_o$),
L = pathlength.

Ze'evi simplified this equation using the Kolmogorov spectrum and the Mellin transform (formula 6.5(15) of [Ref.12]) as follow;

$$\sigma_\chi^2(F,\theta=0) = A_1C_n^2\int_0^L dz\left[\frac{z(L-z)}{L}\right]^{5/6}, \quad \text{(eqn 2.13)}$$

where $A_1 = .033(-4)(2^{7/6})\,\Gamma(-5/6)\cos(5\pi/12)\pi^2k^{7/6}$.
Making the transformation by " X = Z/L ", then we get

$$\sigma_\chi^2(F,\theta=0) = A_1L^{11/6}C_n^2\int_0^1 dx\,[x(2-x)]^{5/6}. \quad \text{(eqn 2.14)}$$

The log intensity for the direct path of length L is

$$\sigma_\chi^2(L) = 16\pi^2k^2\int_0^1 dz\int_0^\infty K\phi(K)\sin^2\left[\frac{z(L-z)}{2kL}\right]dK \quad \text{(eqn 2.15)}$$

Using the same steps as in the previous work, we get

Usually we can express the scintillation strength from the normalized variance of the intensity fluctuation, as follows,

$$\sigma_I^2(I/I_c) = \langle (I/I_o)^2 \rangle - \langle I/I_o \rangle^2, \qquad \text{(eqn 2.9)}$$

where I = the intensity at the receiver at time t,

$I_c = \langle I \rangle$

For the case of weak turbulence, it is conventional to calculate the variance of the logarithm of the amplitude fluctuations rather than of the intensity fluctuations. If the log amplitude is normally distributed, the log intensity variance can be shown to be

$$\sigma_\chi^2 = \langle [\ln(I/I_c)]^2 \rangle - \langle \ln(I/I_c) \rangle^2. \qquad \text{(eqn 2.10)}$$

Since the log intensity is proportional to the square of the amplitude, then we have following form;

$$\sigma_\chi^2 = 4 \cdot (0.124\, k^{7/6} L^{11/6} C_n^2). \qquad \text{(eqn 2.11)}$$

This relation is developed by Tatarski [Ref.9] based on the Rytov approximation which gives quiet good agreement for $\sigma_\chi^2 < 0.3$.

E. PATH WEIGHTING FUNCTION

Tatarski showed that for scintillations the weighting of turbulence along the optical path is not uniform. For the case of a reflected spherical wave, the optical scintillation weighting function was investigated by Ze'evi in his doctoral thesis at NPS. In his work, Dr. Ze'evi assumed a plane mirror as the target and a weak Kolmogorov turbulence model.

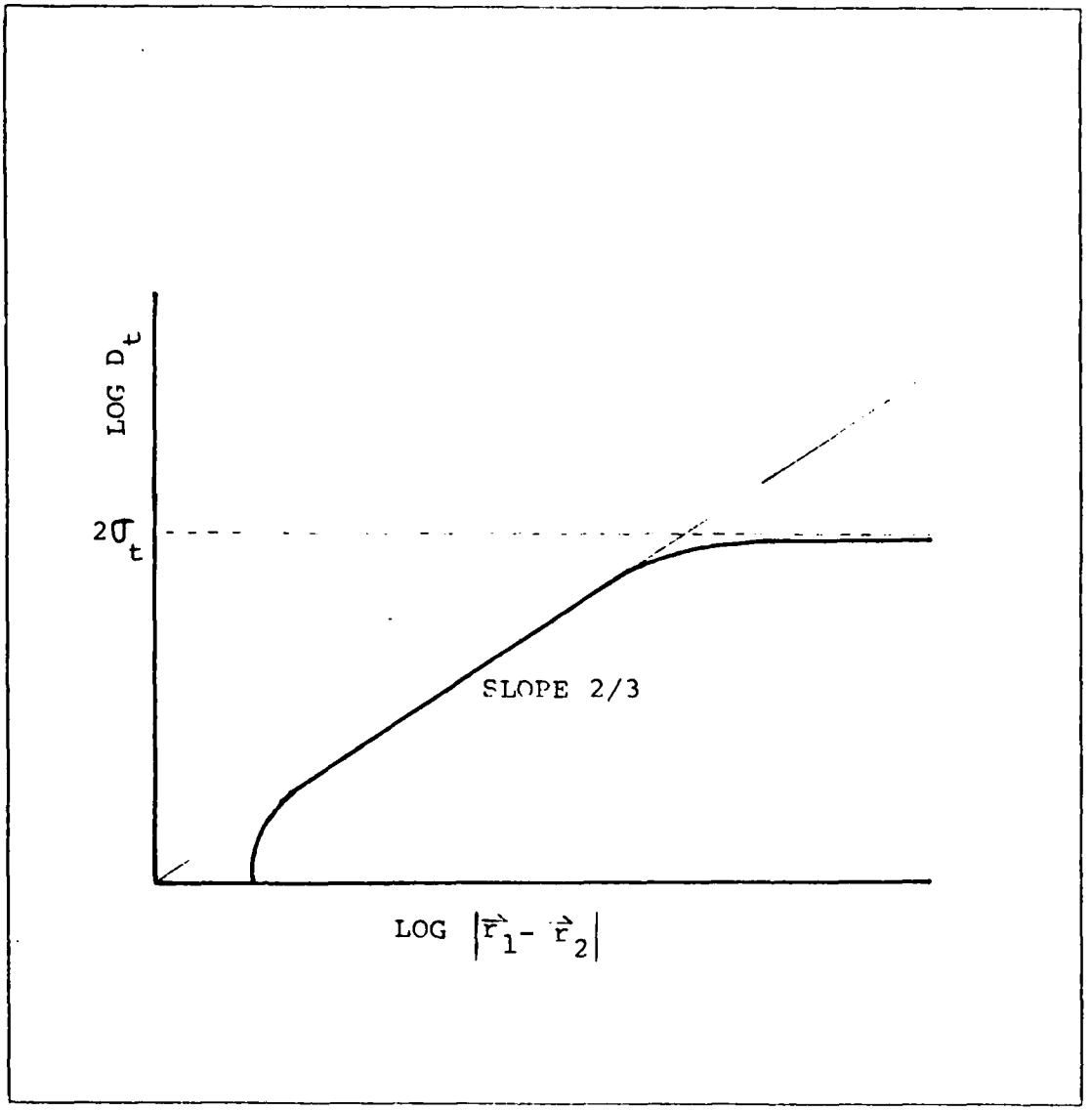

Figure 2.1 Log D_t as a Function of Log $|\vec{r}_1 - \vec{r}_2|$

D. INTENSITY SCINTILLATIONS

We find that the intensity of a beam fluctuates with time about its average value $\langle I \rangle$ in the turbulent medium. The intensity fluctuation can be measured with a detector recording the intensity of the radiation as a function of time.

$$D_t(r) = 2(\langle T^2(\vec{r}_1)\rangle - \langle T(\vec{r}_2)\rangle^2). \qquad \text{(eqn 2.6)}$$

Equation 2.6 shows that the asymptotic limit of $D_t(r)$ is just twice the variance of the temperature fluctuations.

C. AMPLITUDE FLUCTUATIONS

Tatarski [Ref.9] derived the expression of amplitude fluctuations based on a perturbation theory. These theoretical results predict that the amplitude fluctuations at a point increase without bound with increasing propagation distance. For the spherical wave , the log amplitude variance is

$$\sigma_a^2 = 0.124\, k^{7/6} L^{11/6} C_n^2, \qquad \text{(eqn 2.7)}$$

where k is $2\pi/\lambda$ and C_n^2 is the index structure parameter. The index structure parameter can be obtained from the temperature structure parameter C_t^2 .

$$C_n = C_t (79\ P/T^2) \times 10^{-6}, \qquad \text{(eqn 2.8)}$$

where P is the pressure in millibars and T is the temperature in Kelvin.

It has been found experimentally [Ref.10] that Equation 2.7 is valid when the fluctuations are small ($\sigma_a^2 \leq 0.3$) and that the amplitude fluctuations do not increase beyond $\sigma_a^2 \sim 1.0$ with either increasing the path length or turbulence strength.

index structure parameter, C_n^2, which is proportional to the fluctuations of the refractive index.

The structure function of the refractive index in the Kolmogorov inertial subrange is:

$$D_n(n) = \langle [n(\vec{r}_1) - n(\vec{r}_2)]^2 \rangle, \qquad \text{(eqn 2.3)}$$

where $l_o << |\vec{r}_1 - \vec{r}_2| << L_o$,

l_o = the inner scale of turbulence,

L_o = the outer scale of turbulence,

$[n(\vec{r}_1) - n(\vec{r}_2)]$ = difference of refraction, index between position $\vec{r}_1$ and $\vec{r}_2$.

B. TEMPERATURE STRUCTURE FUNCTION

The temperature structure function is

$$D_t(\vec{r}_1 - \vec{r}_2) = \langle [T(\vec{r}_1) - T(\vec{r}_2)]^2 \rangle. \qquad \text{(eqn 2.4)}$$

By dimensional analysis, Kolmogorov showed the structure function for temperature in the Kolmogorov model as follow:

$$D_t(r) = C_t^2 r^{2/3}; \qquad \text{(eqn 2.5)}$$

where $r = |\vec{r}_1 - \vec{r}_2|$ and C_t^2 is the temperature structure parameter. The logarithm of the structure function, $\log D_t$, is shown as a function of $\log |\vec{r}_1 - \vec{r}_2|$ in Figure 2.1

Equation 2.5 is valid as long as r lies between the outer scale and the inner scale of turbulence.

For some larger r, $r > L_o$, the temperature fluctuations become uncorrelated and the structure function asymptotically approaches a limit. For $r \to \infty$, and assuming homogeneity, $\langle T(\vec{r}_1) \rangle = \langle T(\vec{r}_2) \rangle$, and the temperature structure function becomes

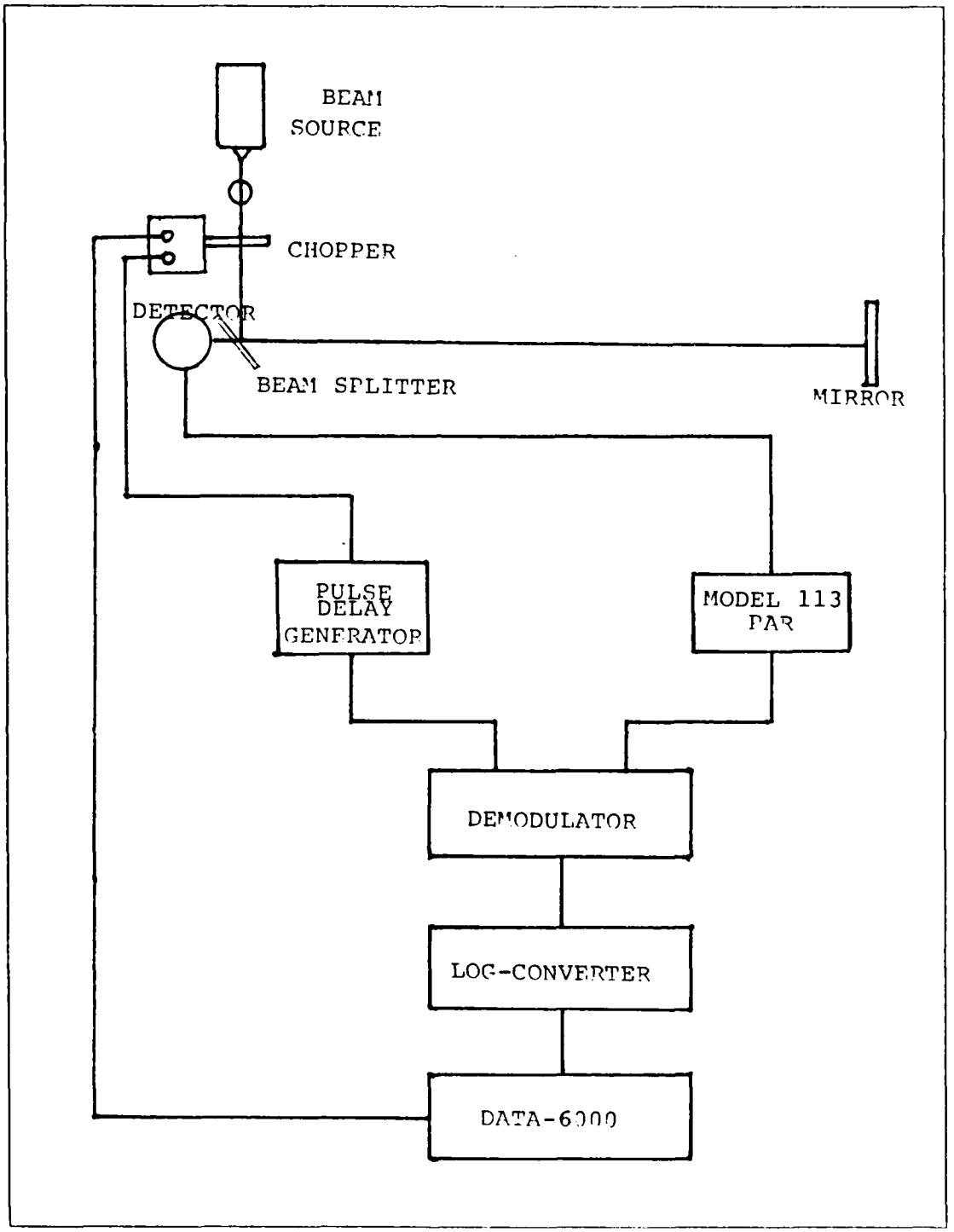

Figure 3.4 Experimental Set Up for the Folded Path.

IV. EXPERIMENTAL WORK

A. GOALS

There were three main goals in our experiment. We continued essentially the same experiment as the work of Constantine [Ref.3] and Henry [Ref.5] with the following goals in mind.

First, to create turbulence in a controlled region that approximated the Kolmogorov spectrum.

Second, to prove or disprove Ze'evi's weighting function for the folded path experimentally.

Third, to compare the results using three different kinds of reflectors (corner cube, flat mirror, cat's eye).

The corner cube had been chosen by Henry because of it's complicated reflection pattern. Additionally, we employed the cat's eye because of it's low reflection.

B. PROCEDURE

In order to achieve Kolmogorov turbulence in the chamber, many runs were conducted in the basement of Spanagel Hall. After assembling the whole experimental system on the roof of Spanagel Hall, we retested the turbulence chamber and obtained the same results that we obtained in the basement to verify the region of the Kolmogorov inertial subrange.

All optical equipment were taped to the concrete floor and the reflector was on an optical bench which was anchored with lead bricks for stability. The tunnel sections were also anchored with lead bricks for wind stability.

We performed the experiments after dark in order to reduce the turbulence in the tunnel caused by the sun heating the tunnel. This also reduced the noise caused by light leaks in the tunnel. The tunnel sections were taped to prevent wind disturbances.

The quiet tunnel scintillation was measured for a reference before we turned on the heater. The scintillation and the variance of temperature fluctuations were measured simultaneously by the DATA-6000 waveform analyzer. The average temperature inside the tunnel was measureed by a copper constantan thermocouple using an ice water reference. The turbulence was then relocated along the path and retaped. This procedure was repeated for each data point.

The DATA-6000 calculated the log intensity variance which was then recorded on magnetic tape by the HP 9825A calculator.

The log intensity variance of the quiet tunnel was subtracted from the log intensity variance at each point. This difference of the variances was then normalized by a factor of $[T^4*<C_t^2>]/[C_t^2*<T^4>]$. The T and C_t^2 are the temperature and temperature structure constant at the point respectively, < > is the ensemble average of the variable over the path. These normalized variances were plotted versus path position.

C. EXPERIMENT

In this section, we discuss briefly the experimental measurements discussed in detail by Mr. Kim [Ref.7]. present the experimental details in his paper. We employed three different kinds of reflectors, (corner cube, flat mirror, and cat's eye), performed experiments for each reflector, and compared the results each other. We first

tried to measure the scintillation for the three reflectors during the same runs. By placing the reflectors on an optical bench, we could change a reflector quickly. During the experiment, the alignment of the flat mirror was destroyed when we changed to another reflector even though the change was made carefully. Additionally we observed an interference pattern on the detector face. So we attached a small black tape to intercept the secondary beam off the back face of the splitter. Finally, we decided to make measurements on the reflectors separately. Because of the problem of interference from multiple reflections, we made a screen in the detector's back board to observe the reflected beam structure at the detector. Since intensity saturation was also observed we decided to employ a convex lens between the source and the chopper. We also observed $\sigma_{\ln A}^2 > .3$, so we reduced the power to the heater in the turbulence chamber. Because of outdoor work, the experiments had to be taken during a calm night. We choose the turbulence location at 1.1, 8.42, 15.74, 23.06, 30.38, 37.70, 42.58, 47.46, 52.34, and 57.22 meters along the path position. The data collected involved 5 sets of 2500 samples each for each turbulence location. The data was then processed and plotted as discussed in the previous section.

1. Corner Cube

We took data on 11 Oct, 12 Oct, and 17 Oct. The lower power was used for the heater. We retaped the whole tunnel before making each experimental run. After the first run we added the baffles at both sides of the heat source and at the slits of the turbulence chamber to limit unwanted drafts through the turbulence chamber. Figure 4.1, Figure 4.2, Figure 4.3 show the plot of the results. The scintillations had an unexpected increase near the reflector end of the tunnel. The data are listed in Appendix A.

2. Flat Mirror

The experiments for the flat mirror were taken on 20 Oct, 22 Oct, and 24 Oct at night. The weather was clear with a light breeze.

We rechecked all of the equipment and the tunnel section but couldn't find any problems. The scintillation still increased near the vicinity of the reflector but more strongly than the corner cube as shown in Figure 4.4, Figure 4.5, Figure 4.6, and the data in Appendix B.

3. Cat's Eye

It took many trials to align the cat's eye because the beam returned from the Cat's eye appeared to have interference-fringe bands on the order of 5 mm wide at the detector plane, and the intensity of the returned beam was low. Therefore we removed the convex lens from the front of the laser to increase the back scattered laser energy and made measurements with the distorted beam structure. During the first run for the cat's eye, we realized the detector and the source were tilted when we moved the turbulence chamber. Therefore we measured scintillation from the 15.74 meter point for the first run. Since the scintillation data for the first two experiments were too low, we increased the power to the heater.

As we can see in Figure 4.7, Figure 4.8, Figure 4.9, the scintillation gradually dropped from the 30.38 meter point to the end position. The detailed results are in Appendix C.

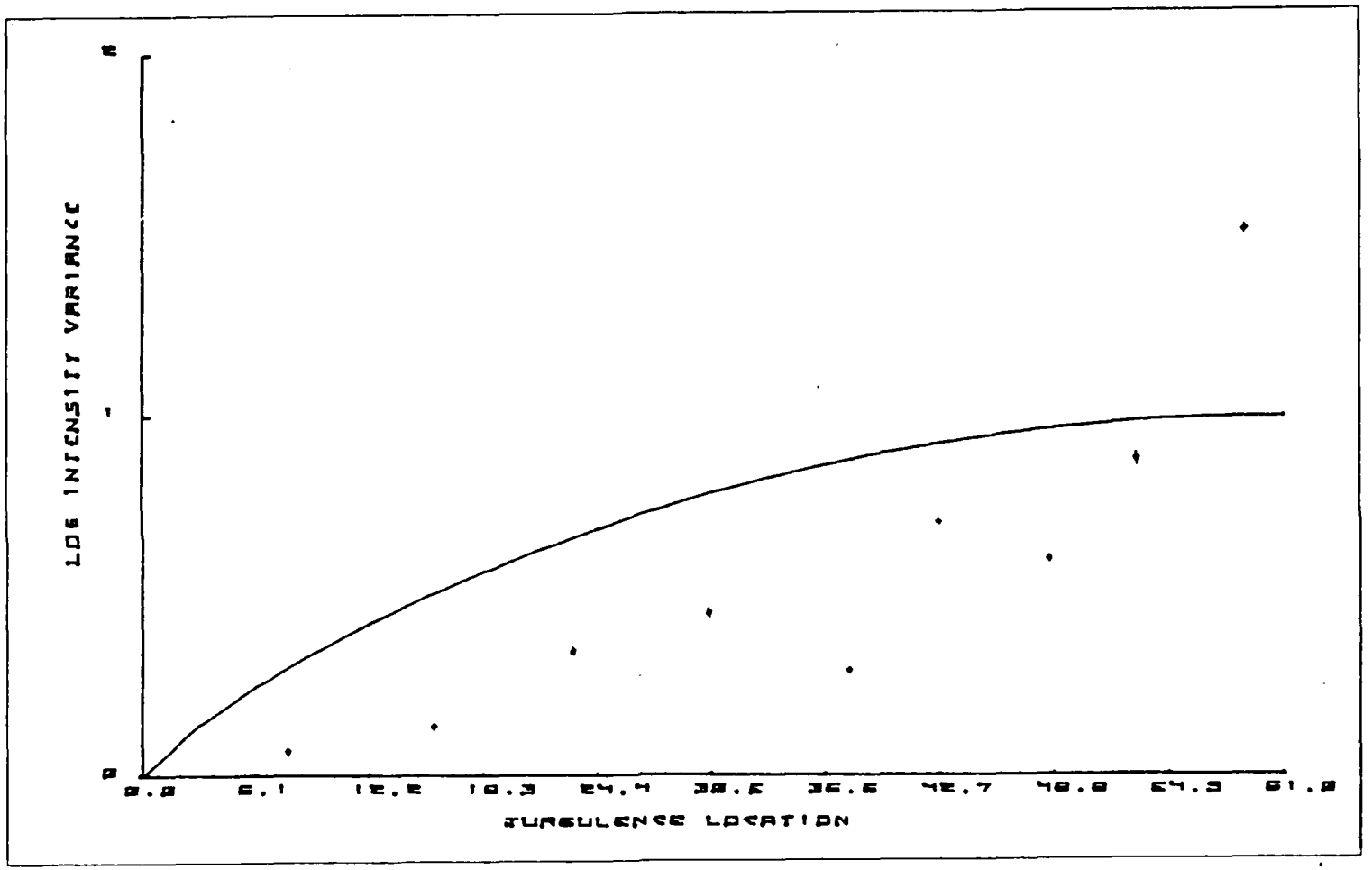

Figure 4.1 Plot for the folded path, corner cube, 11 Oct, 1984. The solid line represents Ze'evi's weighting function.

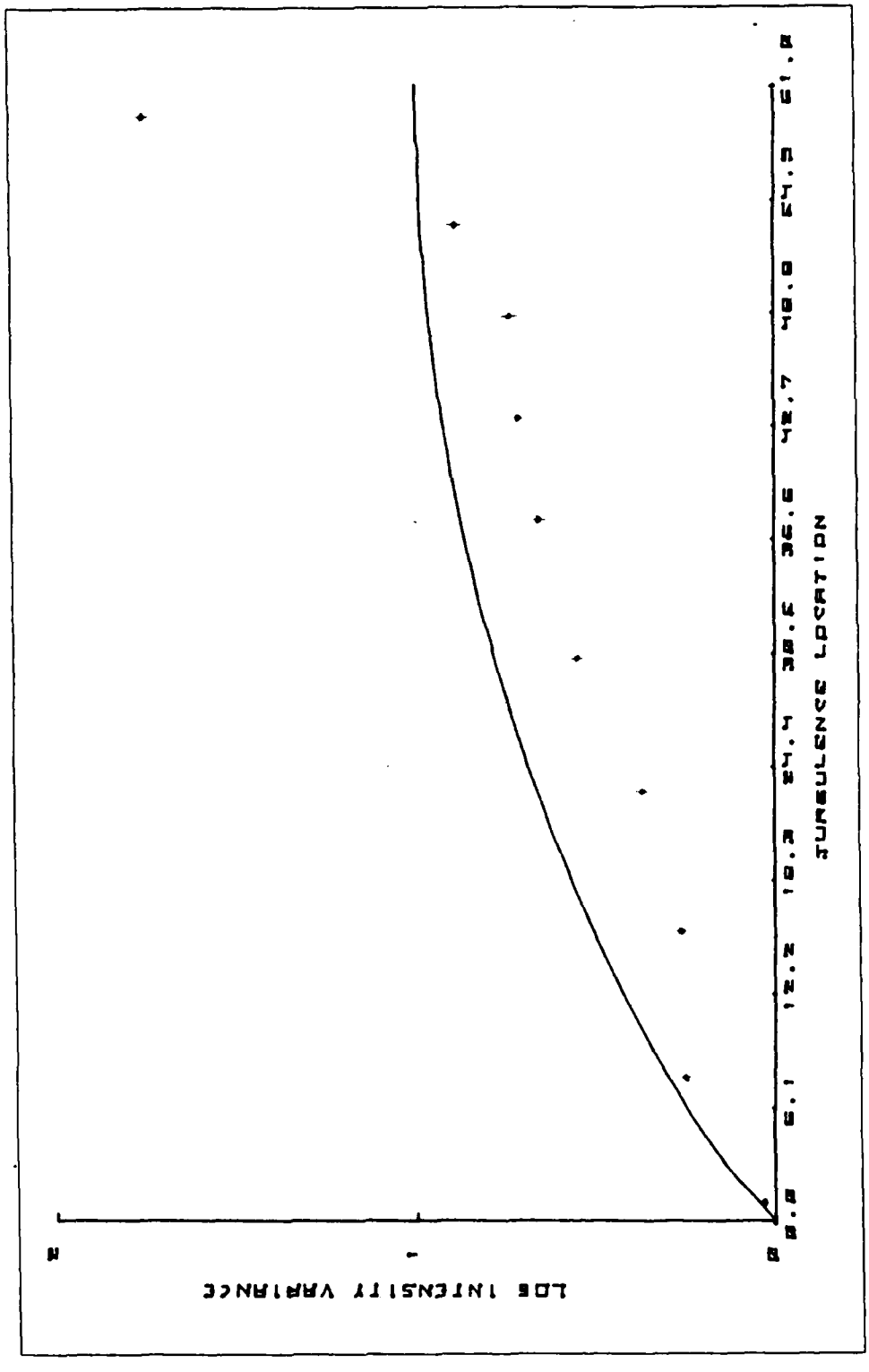

Figure 4.2 Plot for the folded path, corner cube, 12 Oct, 1984. The solid line represents Ze'evi's weighting function.

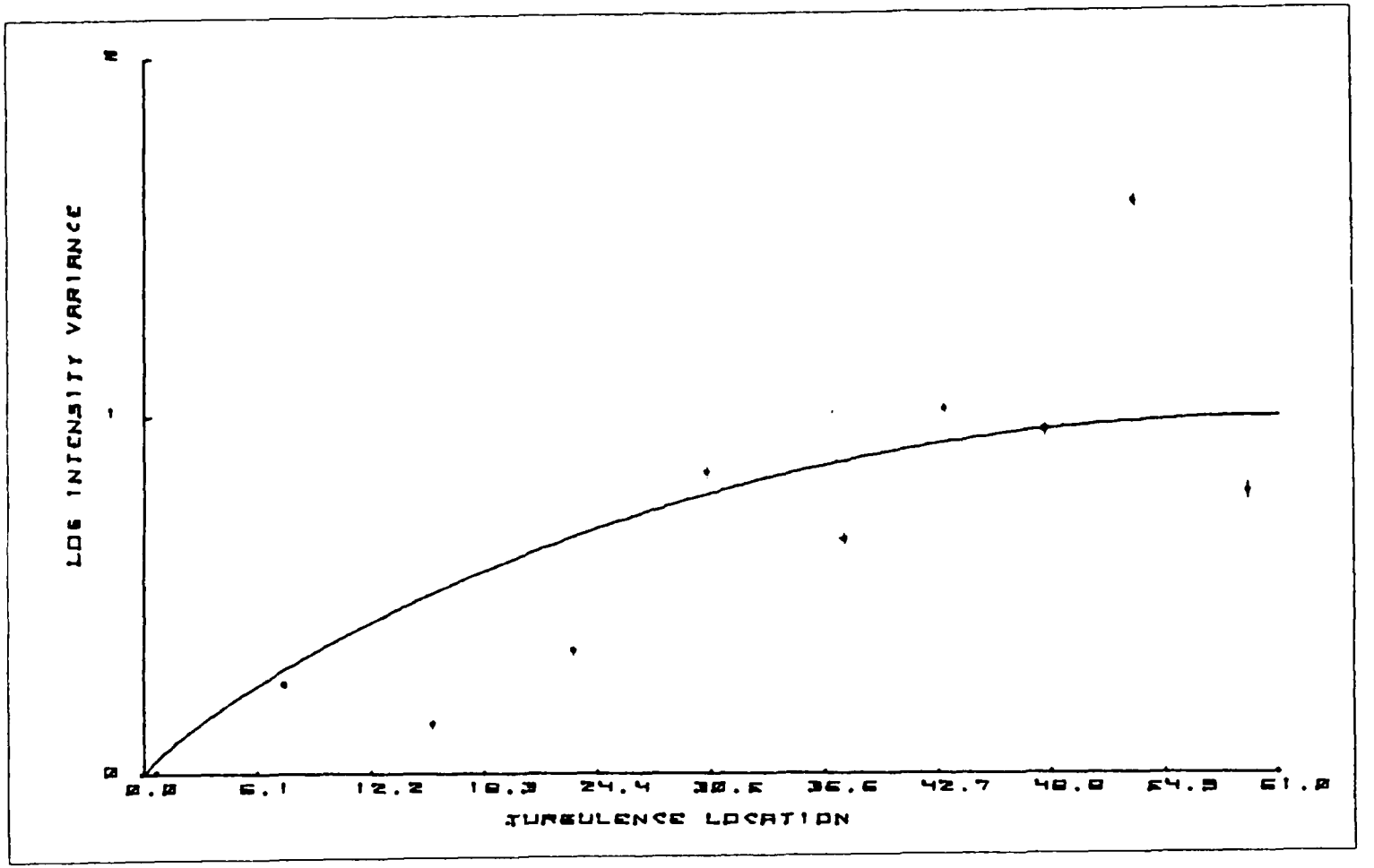

Figure 4.3 Plot for the folded path, corner cube, 17 Oct, 1984. The solid line represents Ze'evi's weighting function.

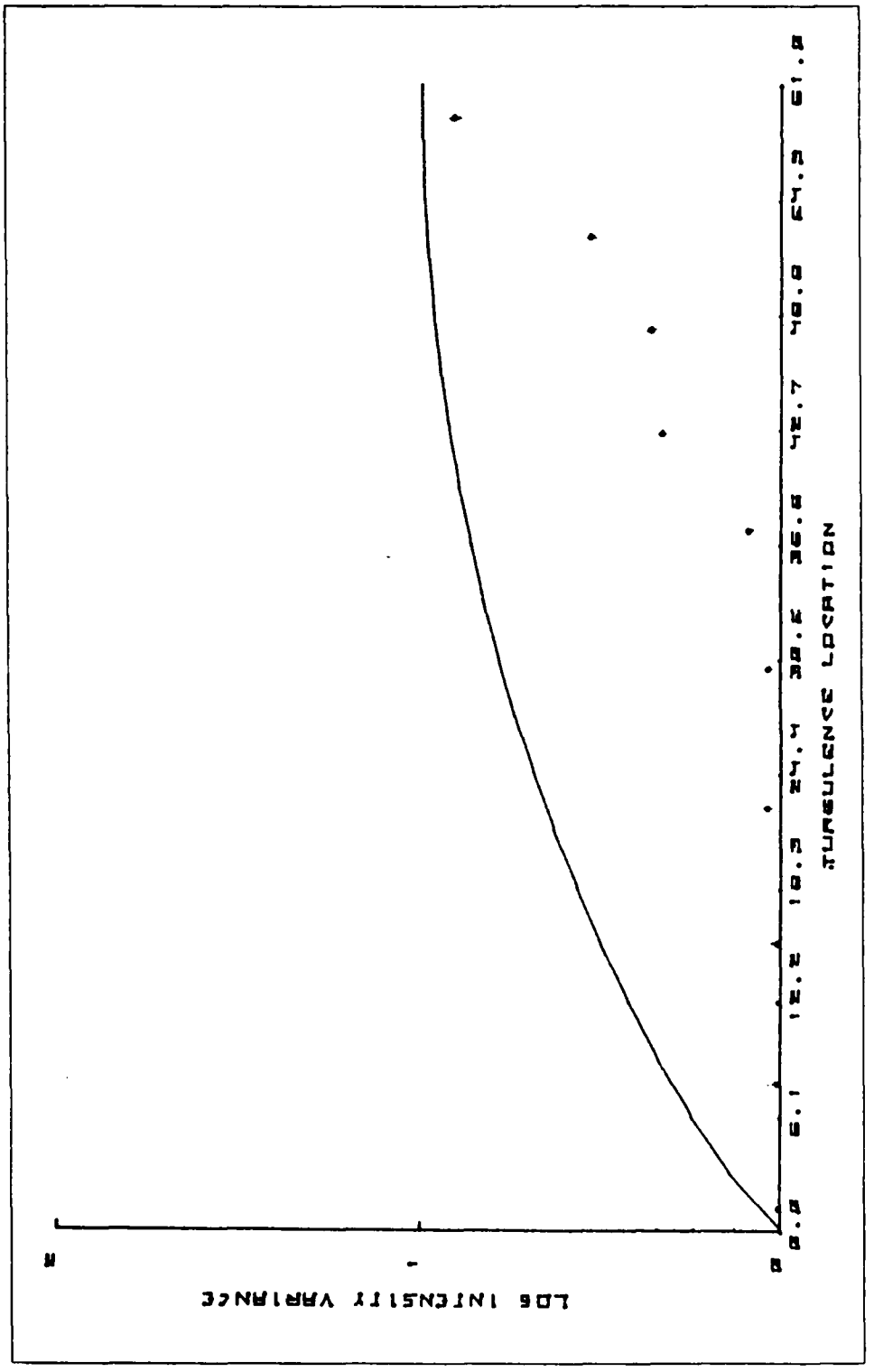

Figure 4.4 Plot for the folded path, flat mirror, 20 Oct, 1984. The solid line represents Ze'evi's weighting function.

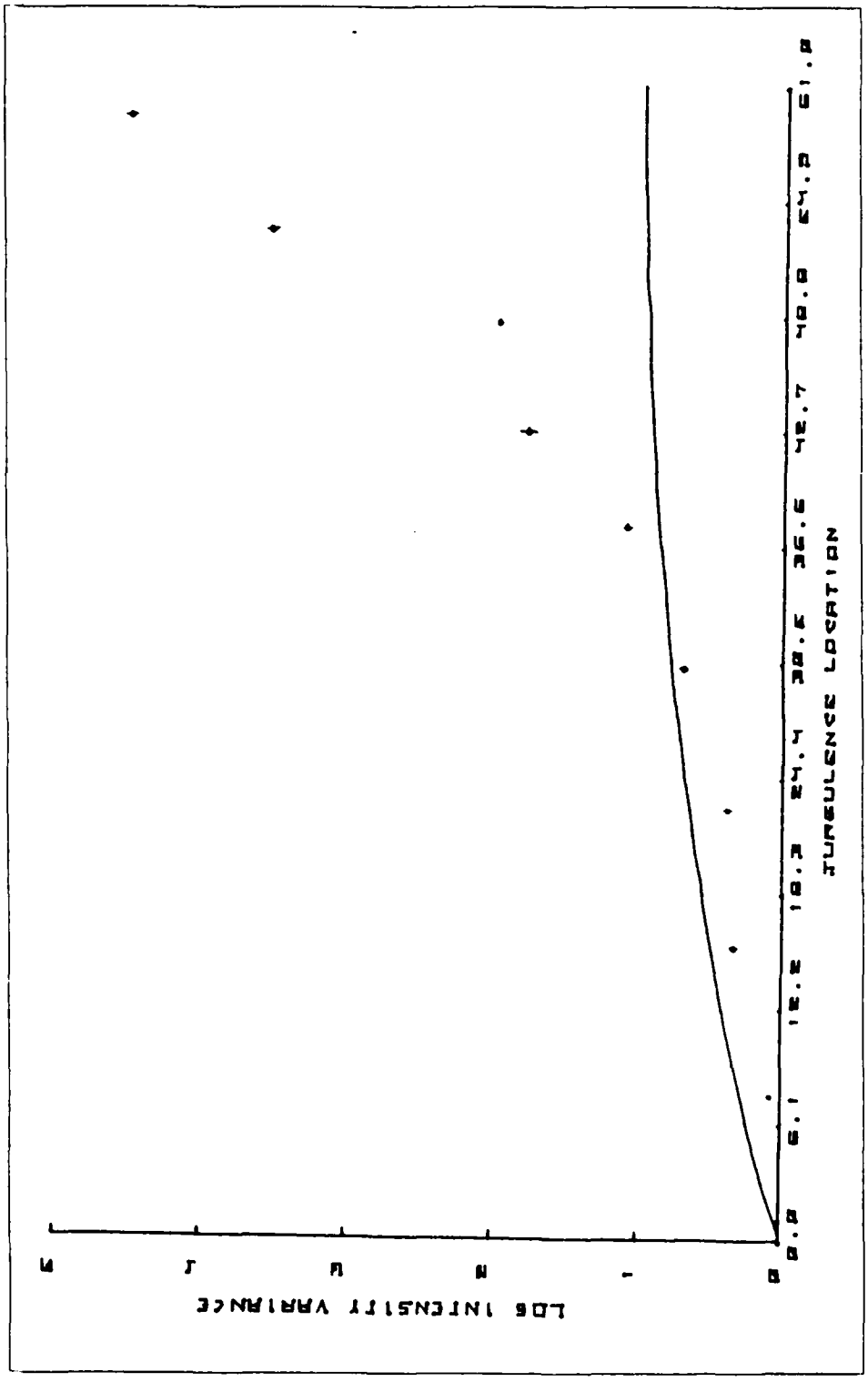

Figure 4.5 Plot for the folded path, flat mirror, 22 Oct, 1984. The solid line represents Ze evi s weighting function.

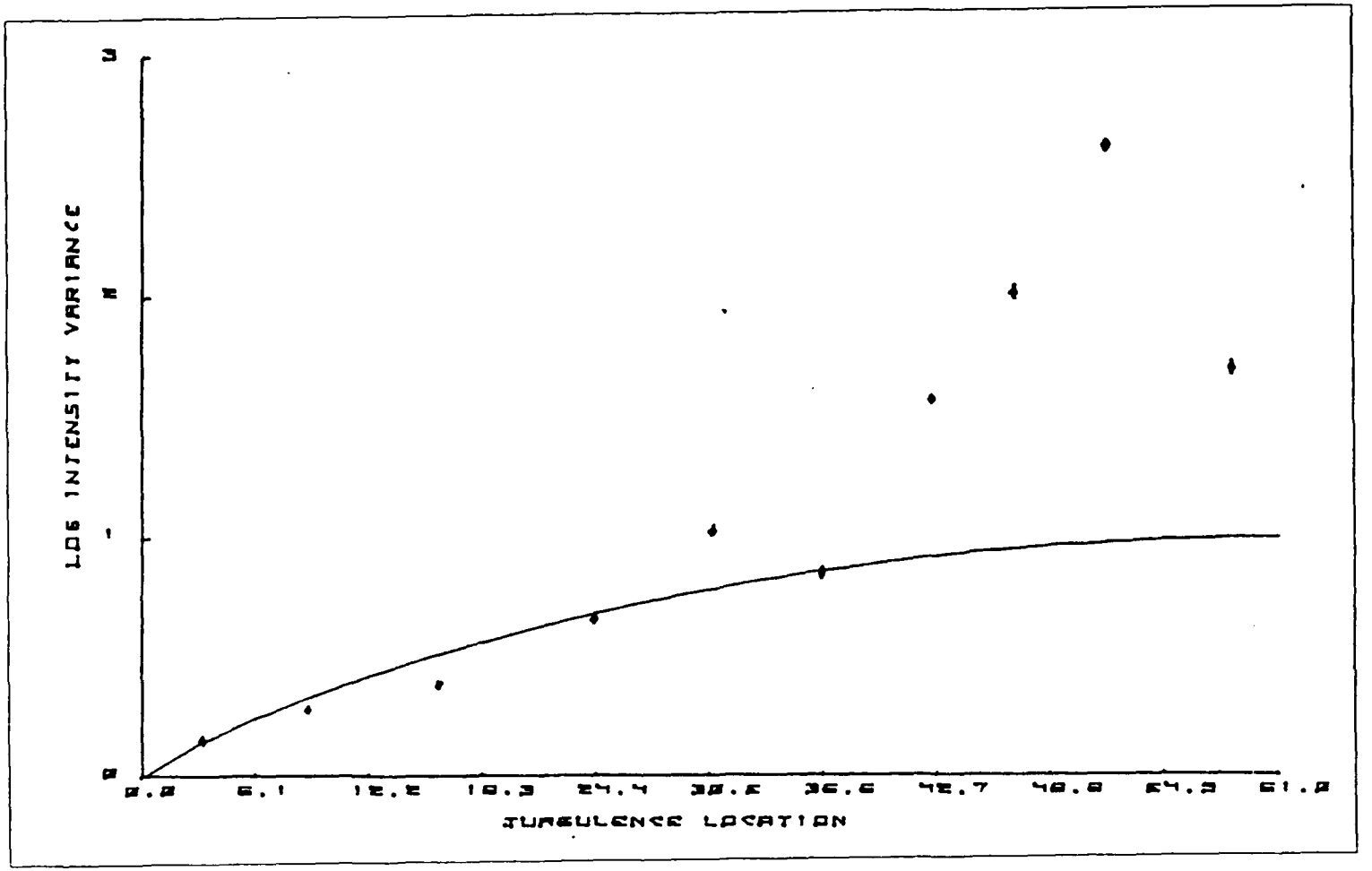

Figure 4.6 Plot for the folded path, flat mirror, 24 Oct, 1984. The solid line represents Ze'evi's weighting function.

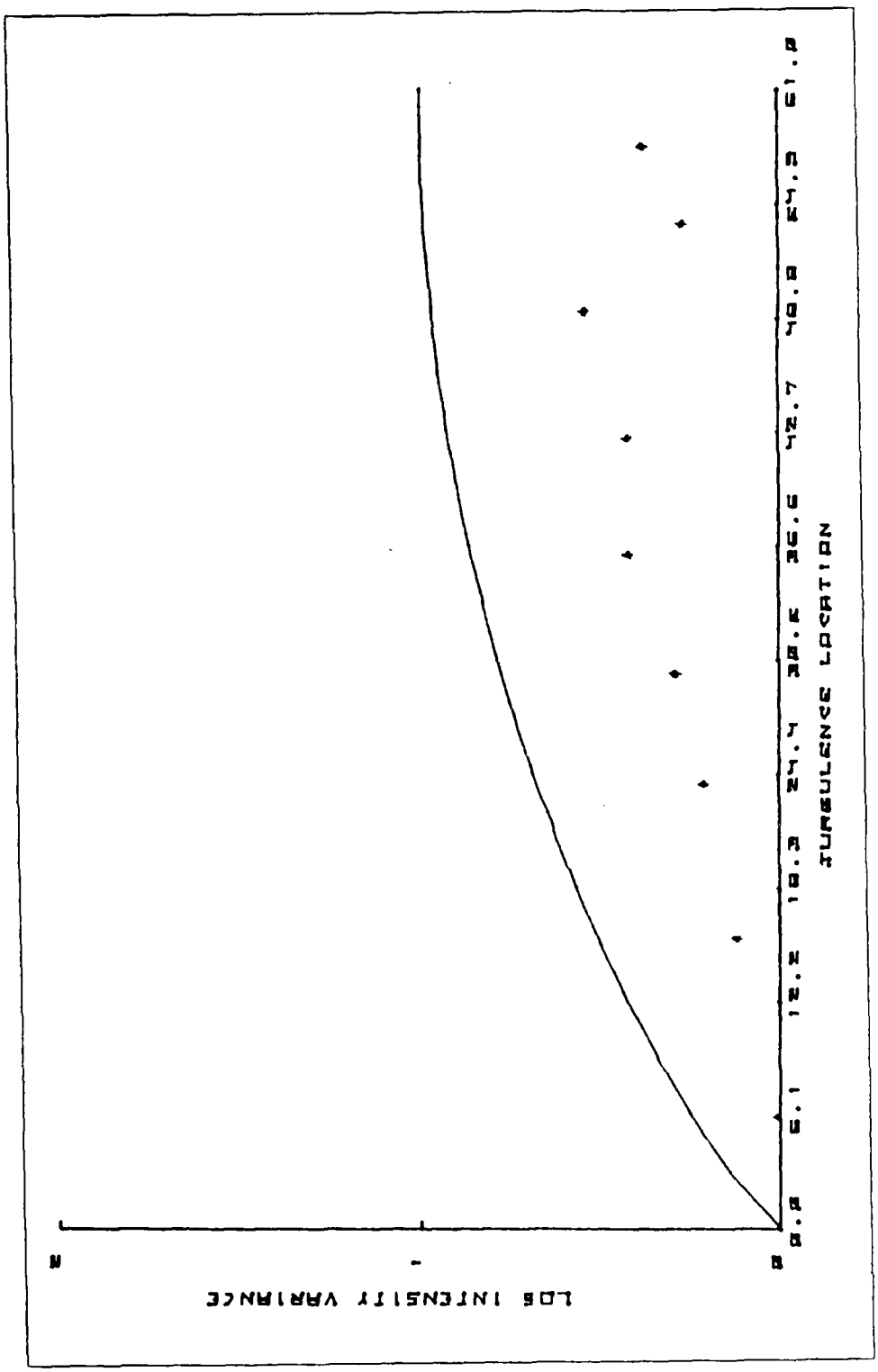

Figure 4.7 Plot for the folded path, cat's eye, 2 Nov. 1984. The solid line represents Ze'evi's weighting function.

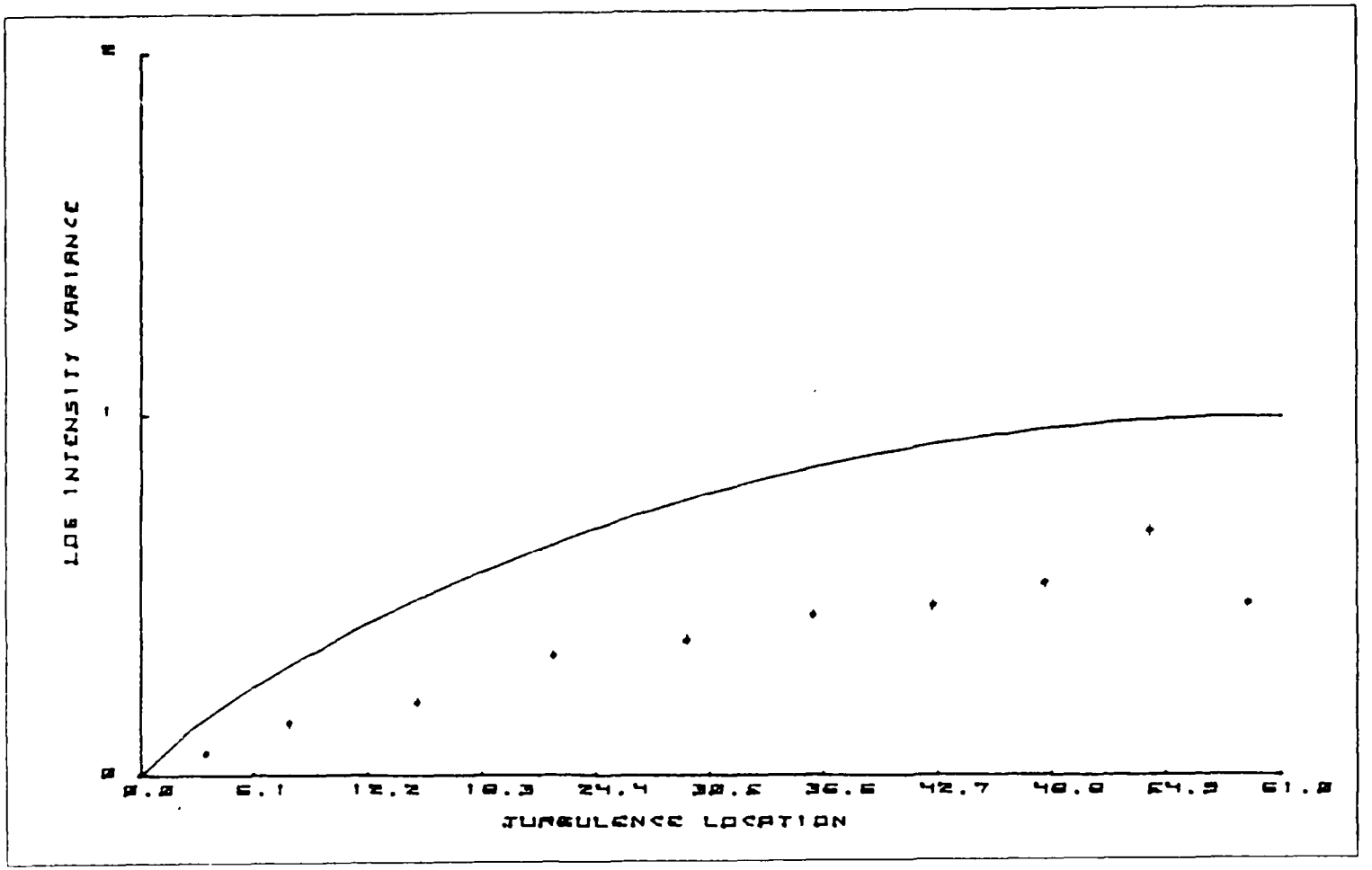

Figure 4.8 Plot for the folded path, cat's eye, 4 Nov. 1984. The solid line represents Ze'evi's weighting function.

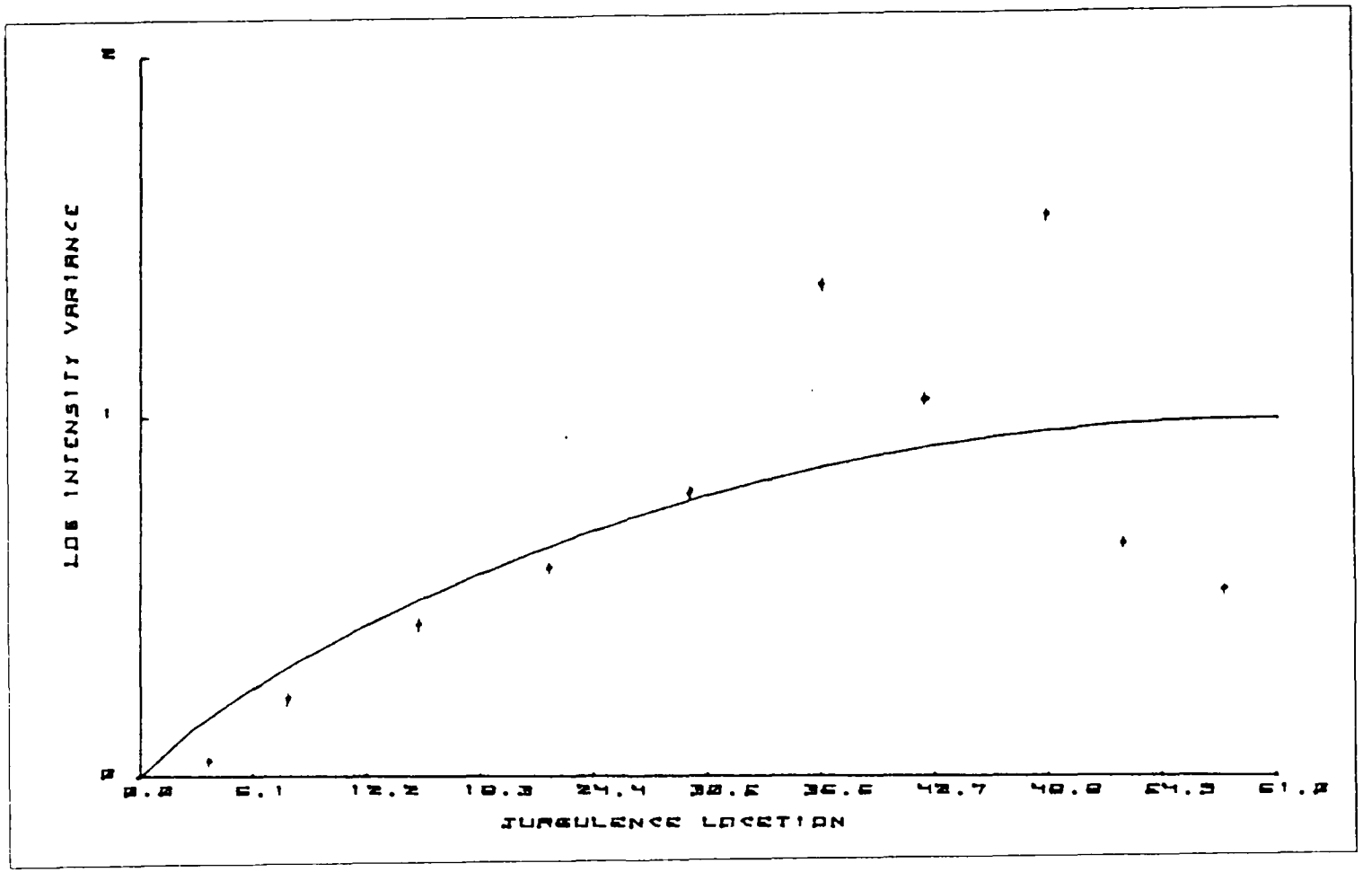

Figure 4.9 Plot for the folded path, cat's eye, 14 Nov. 1984. The solid line represents Ze'evi's weighting function.

DATA OF THE SIXTH EXPERIMENT, 24. OCT. 1984

TURBULENCE LOCATION	$Ct^2 (K^2/m^2)$	$\langle \mathcal{I}_x^2 \rangle$	NORMALIZED LOG-INTENSITY
QUITE		.1675 ± .0005	
1.10	14.99	.1884 ± .0008	1.448 ± .017
8.42	19.98	.2165 ± .0047	2.681 ± .072
15.74	27.07	.2487 ± .0060	3.636 ± .128
23.06	28.47	.2984 ± .0088	6.146 ± .161
30.38	28.37	.3645 ± .0223	10.602 ± .496
37.70	46.95	.4014 ± .0130	8.224 ± .602
42.58	28.98	.4178 ± .0062	14.639 ± .464
47.46	30.77	.4698 ± .0065	18.183 ± .889
52.34	21.02	.4788 ± .0080	26.879 ± .669
57.22	39.93	.4951 ± .0184	15.271 ± .745

DATA OF THE FIFTH EXPERIMENT, 22. OCT. 1984

TURBULENCE LOCATION	$Ct^2 (K^2/m^2)$	$\langle \tau_x^2 \rangle$	NORMALIZED LOG-INTENSITY
QUITE		.1868 ± .0013	
1.10	9.17	.1921 ± .0008	.698 ± .018
8.42	38.11	.2218 ± .0010	1.199 ± .068
15.74	38.84	.2649 ± .0099	2.842 ± .189
23.06	50.16	.3093 ± .0005	3.715 ± .166
30.38	47.30	.3784 ± .0016	6.932 ± .237
37.70	42.03	.4382 ± .0049	11.400 ± .162
42.58	33.48	.4930 ± .0138	19.280 ± .926
47.46	24.98	.4445 ± .0023	20.180 ± .513
52.34	14.34	.4651 ± .0101	38.690 ± .800
57.22	11.19	.4540 ± .0070	46.530 ± .753

APPENDIX B

FLAT MIRROR

DATA OF THE FOURTH EXPERIMENT, 20. OCT. 1984

TURBULENCE LOCATION	$Ct^2 (K^2/m^2)$	$\langle \sigma_\chi^2 \rangle$	NORMALIZED LOG-INTENSITY
QUITE		.1887 ± .0010	
1.10	14.37	.1907 ± .0005	.238 ± .011
8.42	66.35	.2141 ± .0005	.566 ± .025
15.74	40.84	.2529 ± .0001	2.515 ± .181
23.06	35.98	.2914 ± .0049	4.888 ± .268
30.38	94.59	.3770 ± .0129	4.051 ± .416
37.70	42.96	.4376 ± .0011	12.980 ± .489
42.58	17.17	.4292 ± .0156	30.230 ± .411
47.46	20.89	.4877 ± .0187	34.780 ± .659
52.34	17.41	.5246 ± .0088	49.070 ± .615
57.22	7.60	.4830 ± .0527	91.460± 1.270

DATA OF THE THIRD EXPERIMENT, 17. OCT. 1984

TURBULENCE LOCATION	$Ct^2 (K^2/m^2)$	$\langle \sigma_\chi^2 \rangle$	NORMALIZED LOG-INTENSITY
QUITE		.0577 ± .0050	
1.10	9.66	.0607 ± .0022	.088 ± .009
8.42	12.51	.1267 ± .0003	2.535 ± .115
15.74	57.86	.1840 ± .0057	1.319 ± .162
23.06	41.47	.2390 ± .0104	3.200 ± .145
30.38	19.61	.2668 ± .0026	8.385 ± .161
37.70	27.03	.2763 ± .0106	6.569 ± .338
42.58	10.90	.2276 ± .0023	10.603 ± .056
47.46	25.37	.3290 ± .0070	9.810 ± .281
52.34	10.55	.2747 ± .0017	16.100 ± .116
57.22	28.08	.3141 ± .0158	7.897 ± .416

DATA OF THE SECOND EXPERIMENT, 12. OCT. 1984

TURBULENCE LOCATION	$Ct^2 (K^2/m^2)$	$\langle \chi^2 \rangle$	NORMALIZED LOG-INTENSITY
QUITE		.0477 ± .0002	
1.10	20.74	.0629 ± .0021	.355 ± .001
8.42	24.25	.1245 ± .0219	2.407 ± .121
15.74	52.52	.1841 ± .0025	2.624 ± .130
23.06	58.54	.2278 ± .0074	3.663 ± .206
30.38	67.69	.2954 ± .0145	5.446 ± .217
37.70	48.99	.2737 ± .0093	6.503 ± .227
42.58	52.19	.2954 ± .0005	7.165 ± .159
47.46	53.24	.3014 ± .0083	7.343 ± .233
52.34	44.03	.3005 ± .0100	8.993 ± .374
57.22	15.97	.2576 ± .0146	17.770 ± .329

APPENDIX A
CORNER CUBE

DATA OF THE FIRST EXPERIMENT, 11. OCT. 1984

TURBULENCE LOCATION	$Ct^2 (K^2/m^2)$	$\langle \sigma_x^2 \rangle$	NORMALIZED LOG-INTENSITY
QUITE		.1227 ± .0039	
8.42	25.41	.1488 ± .0013	1.106 ± .058
15.74	35.31	.1820 ± .0015	2.176 ± .052
23.06	31.91	.2011 ± .0060	3.205 ± .102
30.38	38.77	.2434 ± .0034	4.558 ± .143
37.70	81.73	.2721 ± .0019	2.863 ± .085
42.58	38.22	.2901 ± .0071	7.054 ± .135
47.46	61.03	.3363 ± .0062	5.925 ± .152
52.34	28.54	.2825 ± .0019	8.797 ± .409
57.22	9.77	.2296 ± .0073	15.160 ± .124

67.5 mm. These eddies have much larger diameter than the Fresnel-zone eddies for the 61 meter tunnel. It is clear that these eddies do not produce strong scintillation in the short path position as we discussed in the section 5.1.

In our experimental results, most of the measured scintillation from 1.1 m to the midpoint of the tunnel showed lower values of scintillation than the theoretical values as we can see from the figures in chapter 4.

The strong scintillation results near the reflector can be explained as follows:

First, the size of the Fresnel-zone at the 30 m position is around 7.5 mm. This is of the order of the inner scale of our turbulence. Therefore, from the 30 m path position, we can consider that Fresnel-size-zone eddies exist along the path position and they contributed to the scintillation at the detector. Second, we must also consider the intensity of the reflected beam. As we discussed in the previous section, the beam spreading decreases when the parcel of turbulence is located near the reflector. When the reflector is smaller than the spot size, some portion of the total intensity should be lost. Since the intensity profile at the reflector has bright and dark regions on the order of one Fresnel-zone in diameter and these regions are moving with the turbulent flow, a small reflector will not be fully illiminated. This will induce additional scintillations in the reflected beam.

Having discussed a simple geometric model of turbulence and analysis of our experimental results, we conclude that we are not able to verify the Ze'evi's weighting function for the folded path with a short path length because of the absence of Fresnel-zone-size eddies.

We recomand that the tunnel should be longer to verify the Ze'evi's theory and the reflector must be larger than the size of beam spot.

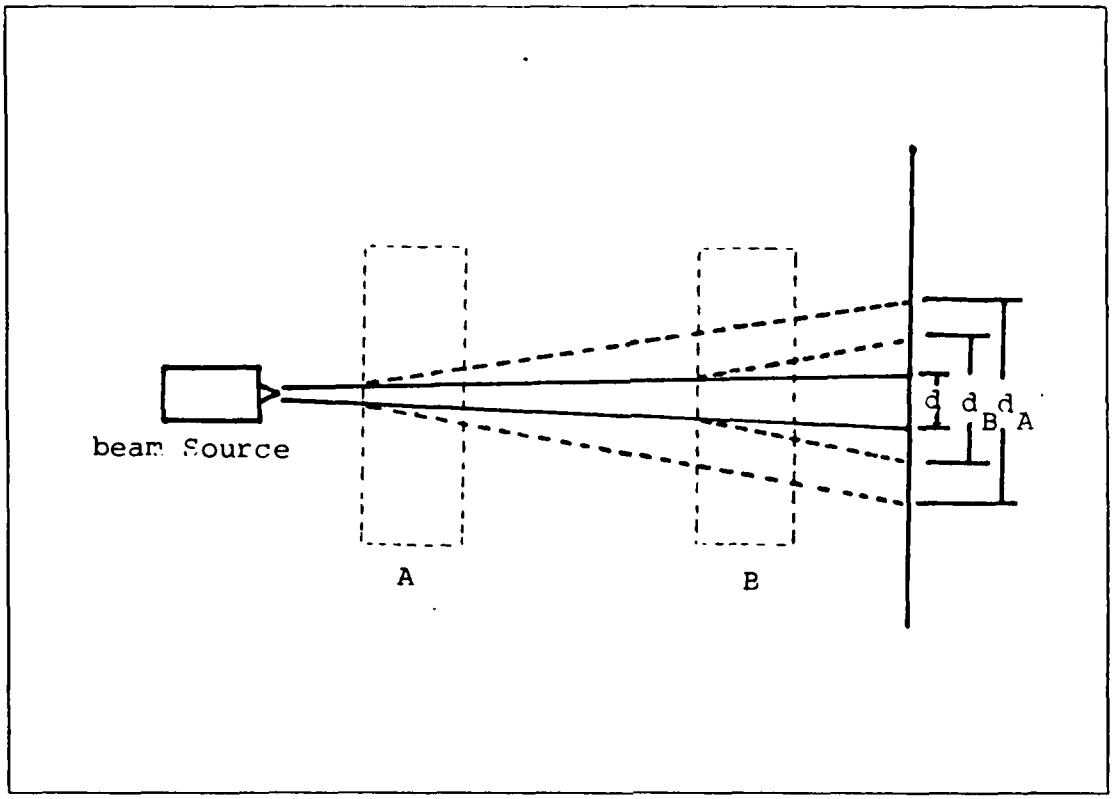

Figure 5.4 The Geometric Figure of Beam Spreading at the Observer Plane.

D. DISCUSSION AND CONCLUSIONS

We have mentioned that the Fresnel-zone-size turbulent eddies along the path can mainly contribute to the scintillation at the detector. That is, the size of the Fresnel-zone-eddy is determined by the path length and by the path position as we saw in equation 5.1

As we can see from the Appendix D, the Fresnel-zone-size eddies have the diameter of 1.4 mm up to 6.6 mm for the direct path and of 1.6 mm up to 8.8 mm for the folded path of the 61 meter tunnel.

From Mr.Lee's works we realized that the inner scale of turbulence in our tunnel is 7.5 mm and the outer scale is

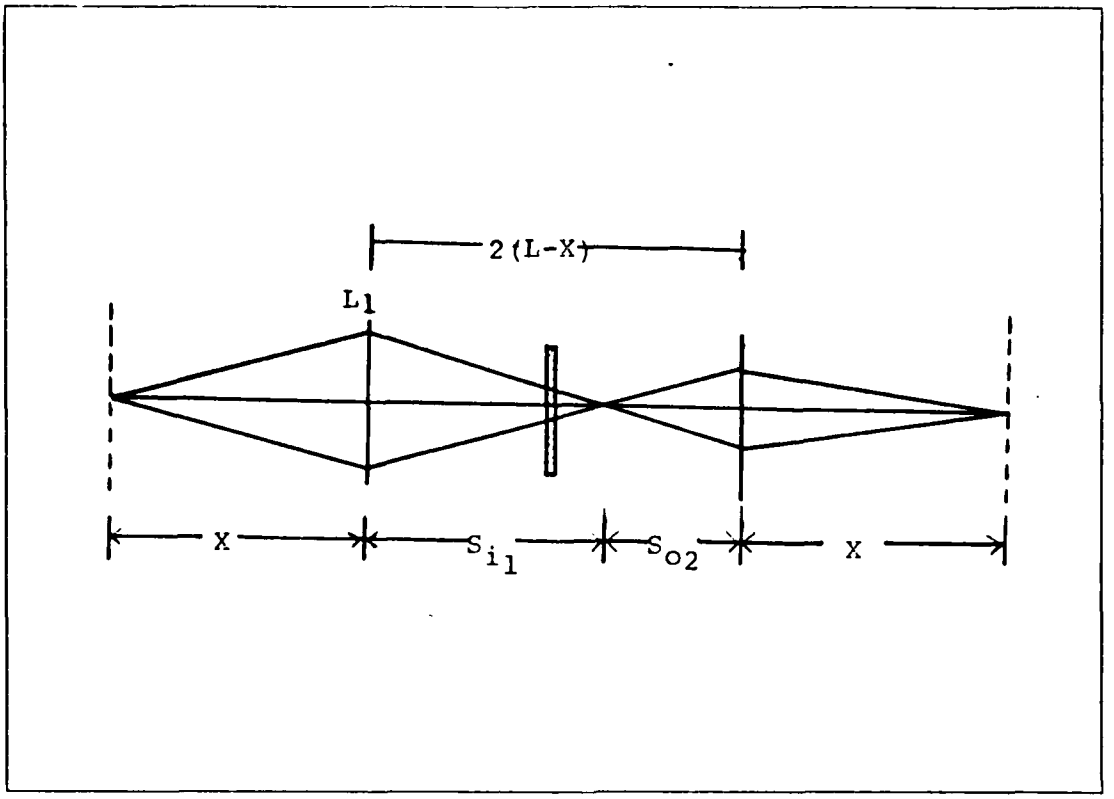

Figure 5.3 The Schematic Geometry of the Two Lens Combination.

arise with angle θ and make a spot of diameter L at observer plane. If, instead, the same parcel of turbulence is located at point B, the beam spreading caused by it will still have the same angle θ, but the spot on the receiving screen will be only d_B in diameter. Thus, if the inherent angular divergence of the laser beam is much smaller than the atmospheric effect, the weighting function that describes the effectiveness for beam spreading of turbulence at various positions along the path is linear. It is a maximum at the source and drops to zero at the observer plane.

From equation 5.2, the image distances from the receiver plane R is

$$d = S_{i_2} - X \qquad \text{(eqn 5.3)}$$

Taking X' = X/L, f' = f/L then equation 5.3 becomes

$$d' = \frac{2f'(1-x') - f'^2x'/(x'-f')}{2(1-x') - f' - f'x'/(x'-f')} - x' \qquad \text{(eqn 5.4)}$$

The numerical values along with the various focal length are listed in Appendix E.

As we can see from the Appendix E, when f < L, the beam focuses at the receiver plane when the turbulent eddy is located at X = f. At f = L, the beam focuses at the receiver plane when the turbulent eddy lens is at the mirror, and with a longer focal lengths than path length L, the beam focuses beyond the receiver plane, if at all. Therefore, in order to focus at the receiver plane the focal length (f) of the eddies must be less than path length (L).

C. BEAM SPREADING

If the laser beam propagates through the random medium, the phase fluctuations in the wavefront will produce a measurable spreading of the beam. The analysis of this effect is surprisingly difficult, though an approximate geometrical solution has been presented by Yura [Ref.14]. Lawrence [Ref.10] explained its approximate nature from the following simple argument. Referring to Figure 5.4, consider a laser source S emitting a well collimated laser of a spot diameter d on the observer plane R. If the parcel of turbulence were inserted in the beam at point A, the beam spreading would

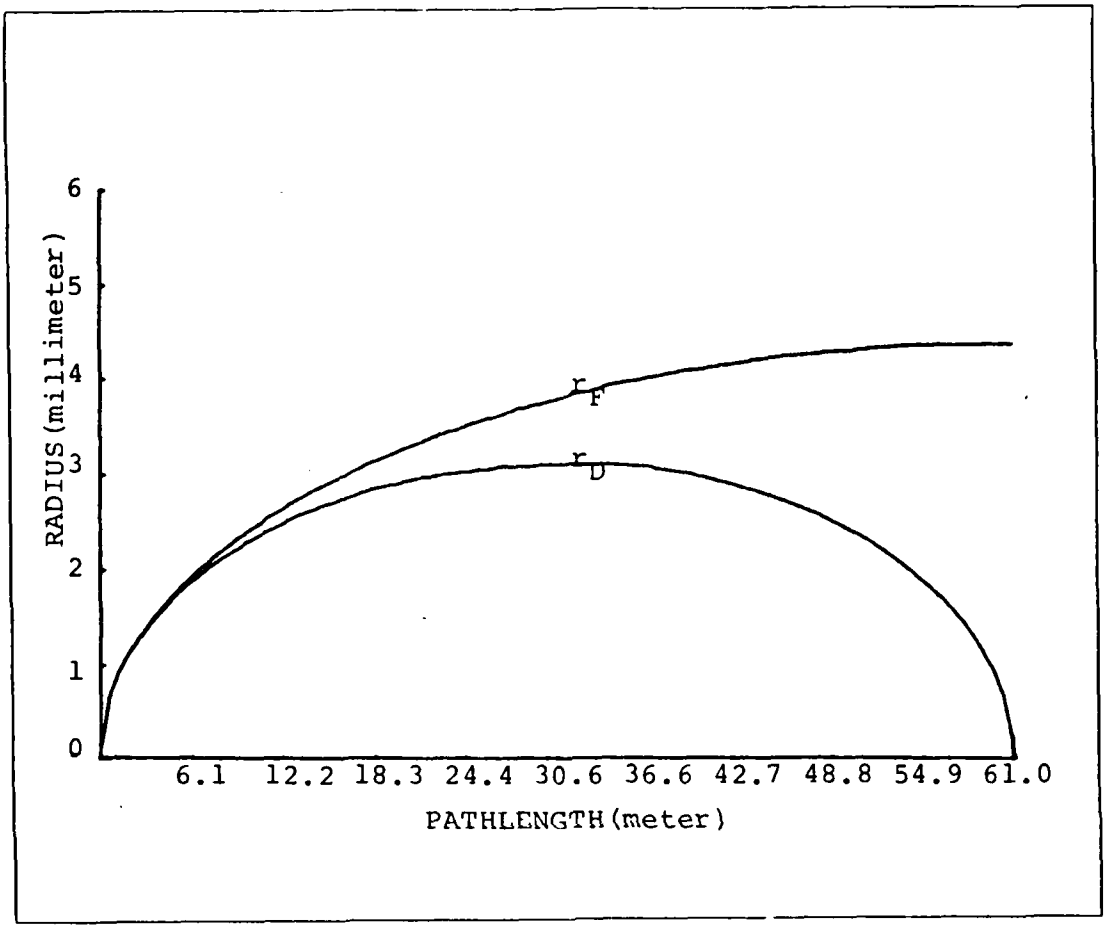

Figure 5.2 The Radius of the Eddy of Fresnel-Zone -Size for Direct Path (r_D) and for Folded Path (r_F) along a 61m Path.

From the Gaussian lens equation the focal points of the eddy lens combination can be obtained.

$$S_{i_2} = \frac{2f(L-X) - f^2X/(X-f)}{2(L-X) - f - fX/(X-f)} \qquad \text{(eqn 5.2)}$$

where S_{i_2} = image point of the eddy lens combination,
f = focal length of the eddy,
L = path length (source to reflector),
X = distance from the source.

the observer plane because of their long focal lengths. Even the smallest details in the scintillation pattern arrive at P unaffected, that is, unsmeared by the large-scale distortions.

The sizes of the Fresnel-zone-eddy along the path length of 61 meters for the direct and for the folded path were plotted in Figure 5.2 for a wavelength of 6328 A. The calculated values are listed in Appendix D.

If we assume that the turbulence has a Kolmogorov spectrum, it is clear that the variance of the refractive-index fluctuations attributable to irregularities of optimum size varies systematically along the path. Consequently the scintillation weighting function is a function of location along the path

From Figure 5.2 it is clear that this weighting function must reach a maximum at the midpoint of the path and for the direct path it has to drop symmetrically to zero at the ends.

Furthermore, the scintillation weighting function assumes that the turbulence has a Kolmogorov spectrum. It is possible for the size of the most effective eddies to be smaller (mm) than the Kolmogorov inner scale.

B. THE FOCAL POINTS OF SINGLE EDDY FOR THE FOLDED PATH

Suppose that the turbulent eddies are two positive lenses of the same focal length (f) and at the distance X from each end. This can be considered as a combination with two turbulent eddy lenses on the direct path. The schematic geometry is shown in Figure 5.3 This model has been over simplified by use of an eddy lens model. (Actually it would be more rigorous to use a set of orthonormal functions to describe the turbulent medium.)

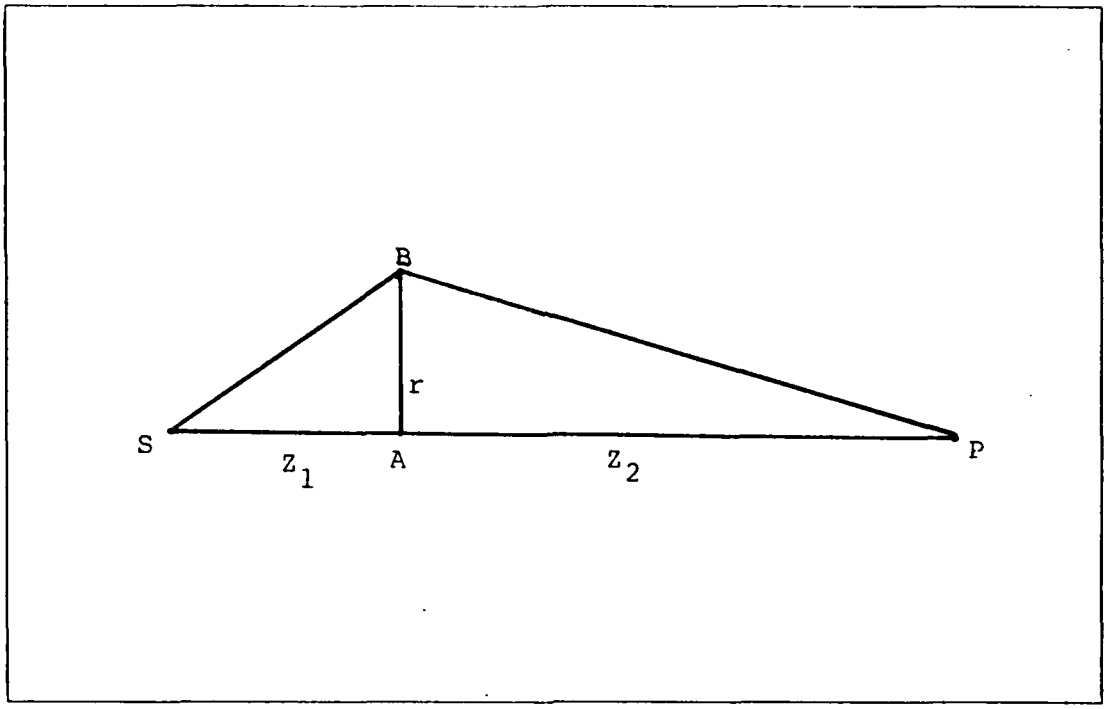

Figure 5.1 The Geometry of the Simple Turbulent Eddy.

is the most effective in producing scintillations at the observer's plane is the one that satisfies the condition SBP - SP = $\lambda/2$, so that the two rays interfere destructively. Working out the geometry of Figure 5.1, Clifford et al [Ref.13] showed that this Fresnel-zone-size eddy has a radius

$$r^2 \sim Z\lambda(1 - Z / L) \qquad \text{(eqn 5.1)}$$

where Z is the distance of the eddy lens from the source and L is the path length.

Let us consider the effects of the various size eddies to the scintillation. Eddies smaller than Fresnel zone contribute less because of the weak refractive fluctuations. Larger eddies also will not produce strong scintillation at

V. DISCUSSION AND OBSERVATIONS

In this chapter, we consider the size of the Fresnel-zone-eddies and then measured the image point of the eddy lens combinations from the detector due to the turbulent eddy location along the path length.

Finally we discuss the experimental results in a view of the above discussed points.

A. GEOMETRICAL MODEL OF TURBULENCE

The physical mechanism by which turbulence induces beam break-up is random focusing of light by refractive inhomogeneities in the path of the optical wave. The geometrical expressions were first developed by Tatarski [Ref.9]. He described the eddies in the atmosphere as spherical lenses whose refractive index is determined by the fluctuation dn, from their surroundings.

Since dn is much less than unity, we can neglect the reflection at the surface of the random medium. Therefore, we did not consider the effects of absorption or scattering by either aerosol or molecules in this paper.

In the paraxial approximation, it is well known that an eddy can act as a lens with a focal length $f = r/dn$ (where r is the radius of eddy). For $dn>0$, the lens is convergent, and for $dn<0$, the lens is divergent. In the atmosphere, the fluctuation dn is much less than 10^{-6}, which implies that $f \geq 10$ Km.

Let's consider the turbulent eddy of radius r in the atmosphere as shown in Figure 5.1. The spherical wave of a wavelength λ encounters a turbulent eddy at position A between source S and the observer's plane P. The eddy that

APPENDIX C
CAT'S EYE

DATA OF THE SEVENTH EXPERIMENT, 2. NOV. 1984

TURBULENCE LOCATION	$Ct^2 (K^2/m^2)$	$\langle \mathcal{J}_1^2 \rangle$	NORMALIZED LOG-INTENSITY
QUITE		.0779 ± .0003	
15.74	39.36	.1510 ± .0049	1.003 ± .044
23.06	31.26	.1701 ± .0083	1.709 ± .125
30.38	39.82	.2120 ± .0016	2.231 ± .086
37.70	24.51	.2037 ± .0213	3.206 ± .227
42.58	15.48	.1701 ± .0031	3.351 ± .089
47.46	11.50	.1705 ± .0078	4.454 ± .140
52.34	10.94	.1336 ± .0049	2.394 ± .065
57.22	8.79	.1339 ± .0021	3.001 ± .050

DATA OF THE EIGHTH EXPERIMENT, 4. NOV. 1984

TURBULENCE LOCATION	$Ct^2 (K^2/m^2)$	$\langle \chi_1^2 \rangle$	NORMALIZED LOG-INTENSITY
QUITE		.1564 ± .0029	
3.55	30.25	.1703 ± .0042	.602 ± .086
8.42	30.33	.1810 ± .0013	1.092 ± .027
15.74	55.25	.2118 ± .0005	1.432 ± .037
23.06	44.28	.2431 ± .0005	3.078 ± .190
30.38	53.09	.2636 ± .0010	3.286 ± .085
37.70	55.78	.2844 ± .0029	3.945 ± .107
42.58	47.25	.2714 ± .0091	4.152 ± .206
47.46	40.44	.2724 ± .0010	4.882 ± .067
52.34	24.84	.2543 ± .0003	6.498 ± .254
57.22	12.96	.1956 ± .0083	4.248 ± .113

DATA OF THE NINTH EXPERIMENT, 11. NOV. 1984

TURBULENCE LOCATION	$Ct^2(K^2/m^2)$	$\langle \overline{J_i}^4 \rangle$	NORMALIZED LOG-INTENSITY
QUITE		.0709 ± .0023	
3.55	233.02	.1250 ± .0029	.471 ± .152
8.42	122.23	.1708 ± .0055	1.999 ± .151
15.74	130.10	.2341 ± .0223	3.975 ± .328
23.06	130.07	.2886 ± .0010	5.912 ± .199
30.38	105.09	.3028 ± .0026	7.974 ± .282
37.70	55.39	.2993 ± .0001	14.425 ± .272
42.58	53.43	.2596 ± .0119	11.390 ± .204
47.46	34.64	.2501 ± .0148	16.122 ± .267
52.34	64.26	.2072 ± .0031	5.741 ± .172
57.22	61.57	.1803 ± .0099	4.385 ± .193

APPENDIX D

FRESNEL-ZONE-SIZE EDDIE'S RADIUS FOR A 61 METER PATH

TURBULENCE LOCATION SOURCE	EDDY RADIUS (millimeter) DIRECT PATH	FOLDED PATH
1.10	.827	.830
8.42	2.143	2.227
15.74	2.718	2.945
23.06	3.013	3.440
30.38	3.106	3.800
37.70	3.018	4.060
42.58	2.853	4.188
47.46	2.582	4.284
52.34	2.168	4.349
57.22	1.498	4.385
60.00	.789	4.392
61.00	.00	4.393

APPENDIX E

POSITION AT FOCAL POINTS MEASURED FROM THE DETECTOR

EDDY LENS POSITION FROM DETECTOR	FOCAL POINTS (λ L) f=.1L	f=.2L	f=.3L	f =.4L	f=.5L	f=.6L
.00	0.11	0.22	0.35	0.50	0.60	0.86
.1L	0.00	0.12	0.25	0.40	0.58	0.79
.2L	-0.09	0.00	0.15	0.30	0.47	0.68
.3L	-0.19	-0.03	0.00	0.17	0.35	0.56
.4L	-0.29	-0.13	-0.40	0.00	0.19	0.40
.5L	-0.39	-0.21	-2.00	-0.21	0.00	0.21
.6L	-0.48	-0.27	-1.20	-0.40	0.19	0.00
.7L	-0.57	-0.17	-0.80	-0.52	-0.35	-0.19
.8L	-0.65	-1.20	-0.74	-0.60	-0.47	-0.34
.9L	-1.01	-0.86	-0.77	-0.69	-0.59	-0.49
Reflector	-0.95	-0.89	-0.75	-0.67	-0.57	-0.46

EDDY LENS POSITION FROM DETECTOR	FOCAL POINTS (λL) f=.7L	f=.8L	f=.9L	f = L	f=1.1L	f=1.2L
.00	1.08	1.33	1.64	2.00	2.44	3.00
.1L	1.00	1.27	1.60	1.99	2.49	3.13
.2L	0.92	1.20	1.55	1.98	2.53	3.25
.3L	0.80	1.09	1.45	1.91	2.50	3.30
.4L	0.64	0.93	1.29	1.75	2.36	3.20
.5L	0.44	0.72	1.06	1.50	2.08	2.89
.6L	0.21	0.47	0.78	1.17	1.69	2.40
.7L	0.00	0.22	0.48	0.82	1.25	1.83
.8L	-0.18	0.00	0.22	0.49	0.84	1.30
.9L	-0.33	-0.18	0.00	0.22	0.50	0.85
Reflector	-0.46	-0.33	-0.18	0.00	0.22	0.50

EDDY LENS POSITION	FOCAL POINTS (λL)					
FROM DETECTOR	f=1.3L	f=1.4L	f=1.5L	f=2L	f=3L	f=4L
.00	3.71	4.67	6.00		-6.00	-4.00
.1L	3.98	5.16	6.93	-40.32	-5.31	-3.73
.2L	4.25	5.72	8.10	-20.70	-4.79	-3.51
.3L	4.45	6.23	9.38	-14.49	-4.41	-3.33
.4L	4.44	6.44	10.27	-11.73	-4.12	-3.19
.5L	4.10	6.09	10.00	-10.50	-3.93	-3.09
.6L	3.45	5.16	8.40	-10.27	-3.81	-3.02
.7L	2.67	3.97	6.25	-11.08	-3.75	-2.97
.8L	1.93	2.86	4.36	-13.80	-3.76	-2.95
.9L	1.33	1.98	2.97	-23.34	-3.84	-2.96
Reflector	0.86	1.33	2.00		-4.00	-3.00

LIST OF REFERENCES

1. Ze'evi, A., Optical Scintillation Along Folded Path, PH.D Thesis, Naval Postgraduate School, Monterey, California, March 1982.

2. Speer,B.A., and Parker, F.H., Measurements of Direct Path and Folded Path Optical Scintillation, Master's thesis, Naval Postgraduate School, Monterey, California, December 1982.

3. Constantine, A.G., Measurements of The Direct Path and Folded Path Optical Scintillation Path Weightings, Master's thesis, Naval Postgraduate School, Monterey, California, June 1983.

4. Flenniken, J.R., Weighting for The Modulation Transfer Function, Master's thesis, Naval Postgraduate School, Monterey, California, June 1983.

5. Henry, L.M., Measurements of The Direct Path and Folded Path Optical Scintillation Using a Corner Cube Reflector, Master's Thesis, Naval Postgraduate School, Monterey, California, December 1983.

6. Lee, J.B., Characterization of the Turbulence in a Turbulent Source Section, Master's thesis, Naval Postgraduate School, Monterey, California, December 1984.

7. Kim, J.H., Measurements of Folded Path Optical Scintillation Using a Corner, a Cat's Eye and a Flat Mirror Reflector, Master's thesis, Naval Postgraduate School, Monterey, California, December 1984.

8. Perkin-Elmer Corporation, Norwalk, CT, Technical Report No. RADC-TR-65-511 Optical Propagation Study, by R.E. Hufnagel, January 1966.

9. Tartarski, V.I., The Effects of the Turbulent Atmosphere on Wave Propagation, Keter Press Binding, 1971.

10. Smith, J., "Folded Path Weighting Function for a High Frequency Spherical Wave," JOSA, vol. 63, p. 1095, 1973.

11. Clifford, S.F., Ochs, G.R., Lawrence, R.S., "Saturation of Optical Scintillation by Strong Turbulence," JOSA, vol. 64, P. 148. 1974.

12. ESSA Research Laboratories Report, Remote Atmospheric Probing by Ground-to-Ground Line-of-Sight Optical Methods, by R.S. Lawrence, 1969.

13. Yura, H.T., "Physical Model for Strong Optical-Amplitude Fluctuation in a Turbulence Medium," JOSA, vol. 64, P. 59, 1974.

14. Bataman Manuscript Project, Tables of Integral Transforms, Ed: Erdelyi, A., California Institution of Technology, McGraw-Hill, 1954.

INITIAL DISTRIBUTION LIST

		No. Copies
1.	Defense Technical Information Center Cameron Station Alexandria, Virginia 22314	2
2.	Library, Code 0142 Naval Postgraduate School Monterey, California 93943	2
3.	G. E. Schacher, Chairman, Code 61Sq Department of Physics Naval Postgraduate School Monterey, California 93943	1
4.	Professor E. A. Milne, Code 61Mn Department of Physics Naval Postgraduate School Monterey, California 93943	4
5.	Professor D. L. Walters, Code 61We Department of Physics Naval Postgraduate School Monterey, California 93943	2
6.	B. G. An 1103 24dong Hyundae Apt Apgujeungdong Kangnamgu Seoul 134 KOREA	3

END

FILMED

5-85

DTIC